Check for updates

Plant, Cell & Environment

WILEY

Plant, Cell & Environment

ORIGINAL ARTICLE

Identification of the ARGONAUTE 1-Enriched sRNomes and Targetomes by Integrated RIP-Seq Data Analysis in *Arabidopsis thaliana*

Zhifang Jiang[1] | Zedi Feng[1] | Yiling Dong[1] | Jia Yao[1] | Xiaoxia Ma[2] | Yijun Meng[1]

[1]College of Life and Environmental Sciences, Hangzhou Normal University, Hangzhou, China | [2]School of Pharmacy, Hangzhou Normal University, Hangzhou, China

Correspondence: Xiaoxia Ma (xiaoma_0910@163.com) | Yijun Meng (mengyijun@zju.edu.cn)

Received: 13 May 2026 | **Revised:** 30 July 2026 | **Accepted:** 9 September 2026

Funding: National Natural Science Foundation of China, Grant/Award Numbers: 32370707, 32070655

Keywords: ARGONAUTE 1 (AGO1) | microRNA (miRNA) | RNA immunoprecipitation (RIP) | small RNA binding site (SBS) | targetome

ABSTRACT

In addition to microRNAs (miRNAs), some small interfering RNAs (siRNAs) such as *trans*-acting siRNAs are also associated with ARGONAUTE 1 (AGO1) for target cleavage in plants. Efficient identification of the AGO1-enriched small RNAs (sRNAs) and their targets became a challenging task. Here, we emphasized the utility of RIP (RNA immunoprecipitation) sequencing in probing the above issue. By analyzing the AGO1-RIP-sRNA-seq data, 42 991, 22 516, 34 555, and 19 754 AGO1-enriched sRNAs were identified from flowers, leaves, roots, and seedlings of *Arabidopsis*, respectively. RIP-RNA-seq of DCL1 and HYL1 enabled us to discover 14 miRNA precursor candidates encoding the AGO1-enriched sRNAs. Second, to reduce the false positive rate of small RNA binding site (SBS) predictions, we focused on the SBSs covered by the AGO1 RIP peaks representing the transcriptome-wide binding regions of this protein. Degradome-based cleavage site mapping enabled us to identify the targetomes of the AGO1-enriched sRNAs in distinct samples. Notably, a great portion of the sRNA–target pairs detected in the wild-type seedlings were absent in the *ago1* mutants. The high AGO1 dependency demonstrated the reliability of our workflow for sRNA target identification. Moreover, GO (Gene Ontology) term enrichment analysis showed that the ecotype- and organ-specific targetomes were functionally related to environmental response and organ development, respectively. Finally, some of the AGO1-enriched sRNAs showed great potential of regulating specific long non-coding RNAs. Together, by employing RIP-seq, our study provided a promising workflow for identification of the AGO1-enriched sRNomes and their targetomes in plants.

1 | Introduction

In plants, small RNAs (sRNAs) have been well-known for their critical functions in the RNA interference (RNAi) pathways that are important for plant development (X. M. Chen 2009). Additionally, the ARGONAUTE (AGO) proteins also play a central role in RNAi (Fang and Qi 2016; H. Zhang et al. 2015). In *Arabidopsis* (*Arabidopsis thaliana*), there are 10 annotated members of the AGO family (Vaucheret 2008). Selective association of the sRNA cargoes with specific AGO proteins will basically determine the RNAi pathways in which the sRNAs are involved. To date, the 5′ terminal nucleotide composition and the sequence length of mature sRNAs, and the secondary structures of their precursors in some cases, have been reported to play a key role in specialization of sRNA-guided AGO

Zhifang Jiang and Zedi Feng contributed equally to this work.

All rights reserved, including rights for text and data mining and training of artificial intelligence technologies or similar technologies.

© 2026 John Wiley & Sons Ltd.

complexes called RNA-induced silencing complexes (RISCs) (Mi et al. 2008; Montgomery et al. 2008; Xiao and MacRae 2022; X. Zhang et al. 2014). Besides, the PIWI and MID domains of the AGO proteins themselves also play a pivotal role in specialized interactions between sRNAs and AGOs (Frank et al. 2012; X. Zhang et al. 2014). Notably, all of the sRNA-mediated regulatory pathways in plants, including transcriptional repression, mRNA cleavage, and translation inhibition, are dependent on sequence complementarity between sRNAs and their targets (Fang and Qi 2016). Thus, the high sequence complementarity of the sRNA–target pairs has been taken into consideration to develop the bioinformatics tools for small RNA binding site (SBS) prediction. However, false positive predictions cannot be avoided unless further supported by experimental evidence.

MicroRNAs (miRNAs) are one of the well-characterized sRNA species in plants. Mature miRNAs are processed from the hairpin-formed (also known as stem-loop-structured) precursors through a DICER-LIKE1 (DCL1)- and HYPONASTIC LEAVES1 (HYL1)-dependent pathway. In many cases, the mature miRNAs are selectively loaded into AGO1, and guide the RISCs to the complementary binding regions for transcript cleavage in the middle sites (Jones-Rhoades et al. 2006; Yu et al. 2026). The RNase H activity of the PIWI domain of AGO1 contributes to the slicer activity of the miRNA-guided RISCs. Notably, some small interfering RNAs (siRNAs) such as *trans*-acting small interfering RNAs (ta-siRNAs) and virus-derived siRNAs (vsiRNAs) have also been demonstrated to be associated with AGO1 for target cleavage (Fang and Qi 2016; Fei et al. 2013), pointing to a quite complicated AGO1-associated sRNA population other than miRNAs. Moreover, the sequencing result of the sRNA population extracted from the immunoprecipitated AGO1 protein revealed abundant unannotated sRNAs (Mi et al. 2008; Wang et al. 2011). Thus, efficient discovery and validation of the novel targets regulated by the AGO1-associated sRNAs has become a challenging task. Modified 5′RACE (rapid amplification of cDNA ends) was employed for fine-scale mapping of the slicing sites within the SBSs (Llave et al. 2002; Mallory et al. 2005). But, it is time-consuming and laborious. Relying on the next-generation sequencing platform, degradome sequencing (degradome-seq) was developed for large-scale identification of the sRNA–target interactions by mapping the degradome signatures to the predicted slicing sites (Y. Meng et al. 2011). Due to the high false positive rate of the predicted SBSs and the non-specific degradome read mapping, however, the reliability of degradome-based validation needs to be further improved.

RNA immunoprecipitation (RIP) is a power tool to detect the RNA fragments, including sRNAs interacting with a specific protein. In the present study, we tried to set up a workflow to efficiently identify the AGO1-enriched sRNA populations (sRNomes) and their targets (targetomes) in *Arabidopsis* by integrated analysis of the RIP sequencing (RIP-seq) data. First, based on the previously reported AGO1-RIP-sRNA-seq data of *Arabidopsis* (Wang et al. 2011), 42 991, 22 516, 34 555, and 19 754 AGO1-enriched sRNAs were identified from flowers, leaves, roots, and seedlings, respectively. Many of the already annotated miRNAs and ta-siRNAs were included in the above identified AGO1-enriched sRNomes. Besides, by analyzing the RIP-RNA-seq data of DCL1 and HYL1, a total of 14 miRNA precursor candidates were discovered. Second, in order to reduce the false positive rate of SBS predictions, we focused on the SBSs covered by the AGO1 RIP peaks representing the transcriptome-wide binding regions of the AGO1 protein. Followed by degradome-based cleavage site mapping, the targetomes regulated by the AGO1-enriched sRNAs were identified in distinct biological samples. Notably, a great portion of the sRNA–target pairs detected in the wild type (WT) seedlings were absent in the *ago1* mutants. The high AGO1 dependency demonstrated the high reliability of our workflow for identification of the targets regulated by the AGO1-enriched sRNAs. Moreover, GO (Gene Ontology) term enrichment analysis showed that the ecotype-specific and the organ-specific targetomes were functionally related to environmental response and organ development, respectively. Finally, some of the AGO1-enriched sRNAs showed great potential of regulating specific long non-coding RNA (lncRNA) targets. Taken together, by employing the RIP-seq data, our workflow provides an efficient way for the identification of the AGO1-enriched sRNomes and their targetomes in plants.

2 | Materials and Methods

2.1 | Plant Materials and Growth Conditions

The seeds of *Arabidopsis*, including wild type of seven ecotypes (Altai-5, Col-0, ICE73, Kas-2, Kondara, Se-0, and Zal-1) and the *ago1* mutants of Col-0, were surface-sterilized in 70% ethanol for 3 min and then in 10% NaClO for 10 min. It was followed by four washes with sterile distilled water. The seeds were sown on the solid Gamborg B5 medium at pH 5.8 under sterile condition. After 2-day incubation at 4°C in darkness, the seeds were germinated in a growth chamber with 16-h light (150 μmol/m^2/s) at 24°C. The 2-week-old seedlings were used for sequencing.

2.2 | Degradome Sequencing and Data Processing

For degradome-seq library construction, 150 ng poly(A)-tailed RNAs were extracted from 20 μg total RNAs through two-round purification by using Dynabeads Oligo (dT)25-61005 (Thermo Fisher, CA, USA). Then, the adapters were ligated to the 5′ ends of the RNA remnants by RNA ligase. Reverse transcription was performed to create the first strands of cDNAs with a random primer. After size selection with AMPure XP beads, the single-stranded cDNAs were PCR amplified to produce the double-stranded cDNAs. Single-end sequencing (50 bp) was performed by LC-Bio (Hangzhou, China) with the Illumina HiSeq. 2500 platform following the vendor's recommended protocol.

FASTX-Toolkit (http://hannonlab.cshl.edu/fastx_toolkit/) was used for adapter trimming and low-quality read removal. The pre-treated degradome sequences from 18 to 25 nt were retained. For a degradome dataset, the expression level of one sequence was normalized by dividing the raw read count of this sequence by the total raw read counts of this dataset, and then multiplied by 10^6. The expression levels normalized in RPM (reads per million) enabled cross-library comparisons.

2.3 | Small RNA Sequencing and Data Processing

TruSeq Small RNA Sample Prep Kit (Illumina, San Diego, USA) was used for sRNA-seq library construction according to the

13653040, 0, Downloaded from https://onlinelibrary.wiley.com/doi/10.1111/pce.70893 by Yijun Meng - Hangzhou Normal University , Wiley Online Library on [16/09/2026]. See the Terms and Conditions (https://onlinelibrary.wiley.com/terms-and-conditions) on Wiley Online Library for rules of use; OA articles are governed by the applicable Creative Commons License

manufacturer's manual. Briefly, the RNAs less than 200 nt were separated from 1 μg total RNAs by polyacrylamide gel electrophoresis, and were ligated to the adapters by T4 RNA ligase at both ends. By using SuperScript II Reverse Transcriptase (Invitrogen, USA), the sRNAs containing the adapters were transcribed to the single-stranded cDNAs. These cDNAs were treated as the PCR templates to generate the double-stranded cDNAs which were then purified by 16% TBE gel electrophoresis. Sequencing was performed by LC-Bio (Hangzhou, China) with the Illumina HiSeq. 2500 platform following the vendor's recommended protocol. For sRNA-seq, there are three biological replicates for each sample. Each biological replicate is prepared by pooled sampling with more than 100 seedlings.

FASTX-Toolkit was used for adapter trimming and low-quality read removal. Then, the pre-treated sRNA sequences ranging from 15 to 45 nt were retained for further analyses. For a sRNA dataset, the expression level of one sequence was normalized as described above.

2.4 | RIP-RNA-Seq of AGO1 and HYL1, and Data Analysis

The 16-day-old WT seedlings of Col-0 were used for the RIP-seq experiments. The seedlings were collected and frozen in liquid nitrogen, and grinded by Tissue Lyser II (Qiagen). The grinded powder was treated with cell lysis buffer. Then, 10% of the lysis sample was used as "input," and 80% named "IP" was subject to immunoprecipitation reaction with the AGO1 (Agrisera, cat. no. AS09 527-100) or HYL1 (Agrisera, cat. no. AS06 136) antibody, and the remaining 10% was incubated with rabbit IgG (Cell Signaling Technology, cat. no. 2729S) as a negative control. The IP results are available in Supporting Information Figure S1. By using TRIzol (Invitrogen, cat. no. 15596018CN), RNAs were extracted from "input" and "IP," respectively. Ribo-off rRNA Depletion Kit (Vazyme, China, cat. no. N409) was used for rRNA removal before sequencing library construction. For the AGO1-RIP-seq experiment without rRNA removal, the RNAs extracted from "input" and "IP" were directly used for library construction. Stranded RNA-seq libraries were constructed by using KC-Digital Stranded mRNA Library Prep Kit for Illumina (Seqhealth, cat. no. DR08502). By labeling the pre-amplified cDNAs with 8-nt unique molecular identifier (UMI), duplication bias introduced during PCR and sequencing steps could be eliminated. The libraries enriched with 200- to 500-bp products were quantified. Finally, paired-end sequencing (PE150) was performed by SeqHealth (Wuhan, China) on Illumina NovaSeq 6000.

Raw sequencing data were pre-treated (removal of the low-quality reads and those contaminated with adapters) by using Trimmomatic (Bolger et al. 2014). Clean Reads were further treated with in-house scripts to eliminate duplication bias introduced during PCR and sequencing based on the UMI tags. The de-duplicated sequences were used for protein binding site identification by mapping them onto the *Arabidopsis* TAIR10-annotated genome (https://www.arabidopsis.org/) (Reiser et al. 2024) using STAR (Dobin et al. 2013) with default parameters. Peak calling was performed by using exomePeak (J. Meng et al. 2014) in the "exon" mode, and RIP peaks were annotated by BEDTools (Quinlan and Hall 2010). The RIP peaks ($p < 0.01$) were annotated with genes if they were entirely resided within the gene bodies. No valid peak was called for "IgG control."

2.5 | Bioinformatics Tools and Data Sources Used in This Study

The software packages include: RNAfold 2.6.3 (Lorenz et al. 2011) for RNA secondary structure prediction; TargetFinder 1.7 (Fahlgren and Carrington 2010) for SBS prediction; degradome-based validation of the sRNA–target pair by mapping the slicing sites in the middle of (from the ninth to the 12th nucleotide) the SBSs (Shao et al. 2013); OmicStudio (Lyu et al. 2023) for GO term enrichment analysis; Cytoscape 3.10.3 (Shannon et al. 2003) for sRNA–target pair visualization; IGV 2.19.4 (Thorvaldsdottir et al. 2013) for AGO1 RIP peak visualization; and Guitar (L. Zhang et al. 2022) for distribution pattern analysis of SBSs and the AGO1 RIP peaks.

The genomic information and gene annotations of *Arabidopsis* were retrieved from The *Arabidopsis* Information Resource, TAIR10 (https://www.arabidopsis.org/) (Reiser et al. 2024). All of the miRNA registries were retrieved from miRBase (release 22; http://www.mirbase.org/) (Kozomara et al. 2019). The lncRNAs were retrieved from CANTATAdb 3.0 (http://yeti.amu.edu.pl/CANTATA/) (Szcześniak and Wanowska 2024) and PscLncRNA (http://ibi.zju.edu.cn/psclncrna/) (Xu et al. 2025). The SNP (single nucleotide polymorphism) information of the six ecotypes (Altai-5, ICE73, Kas-2, Kondara, Se-0, and Zal-1), referenced to Col-0, was retrieved from the *Arabidopsis* 1001 Genomes Project (https://1001genomes.org/) (1001-Alonso-Blanco et al. 2016).

The *TAS* genes mentioned in this paper include 11 TAIR10-annotated ones (*AT2G27400*, *AT1G50055*, *AT2G39675*, *AT2G39681*, *AT3G17185*, *AT5G49615*, *AT3G25795*, *AT1G63080*, *AT1G63130*, *AT1G63150*, and *AT5G57735*) and two recently reported *TAS* candidates (Feng et al. 2024). The publicly available sequencing data include: the AGO1-RIP-sRNA-seq data in GEO (https://www.ncbi.nlm.nih.gov/geo/) (accession ID: GSE28591) (Wang et al. 2011), the organ- and temperature-specific degradome-seq data in SRA (https://www.ncbi.nlm.nih.gov/sra/) (accession ID: SRP117737) (Gyula et al. 2018), and the DCL1 RIP peaks in the Supporting Information Table S3 reported by (Bologna et al. 2026). The sequencing data reported by our group include: the degradome-seq data of the seven *Arabidopsis* ecotypes in SRA (accession ID: PRJNA1229083) (Feng et al. 2026), the degradome-seq data of the *ago1* mutants in SRA (accession ID: PRJNA1441820), the AGO1-RIP-RNA-seq data (without rRNA removal) in SRA (accession ID: PRJNA1480398), the AGO1- and HYL1-RIP-RNA-seq data (rRNA removal) in SRA (accession ID: PRJNA1164813), and the sRNA-seq data of Col-0, *ago1-25* and *ago1-27* in SRA (accession ID: PRJNA1250199).

2.6 | Modified 5′RACE

For mapping the slicing sites in the middle of the SBSs on the target transcripts, modified 5′RACE also called RNA ligase

13653040, 0, Downloaded from https://onlinelibrary.wiley.com/doi/10.1111/pce.70893 by Yijun Meng - Hangzhou Normal University , Wiley Online Library on [16/09/2026]. See the Terms and Conditions (https://onlinelibrary.wiley.com/terms-and-conditions) on Wiley Online Library for rules of use; OA articles are governed by the applicable Creative Commons License

mediated rapid amplification of cDNA ends (RLM-RACE) was performed by using the GeneRacer Kit (Invitrogen, Carlsbad, CA) as described previously (Llave et al. 2002). Briefly, total RNAs were extracted from 16-day-old wild-type seedlings of *Arabidopsis* by using the OminiPlant RNA Kit (DNase I) (CWBIO, Taizhou, China) according to the manufacture's protocol. Poly(A)-tailed mRNAs were purified by using the Dynabeads mRNA Purification Kit (Invitrogen, Vilnius, Lithuania), and then were ligated (250 ng) to the GeneRacer RNA Oligo adapter (5′ CGACUGGAGCACGAGGACACUGACAUGGACUGAAGGAGUAGAAA 3′). The GeneRacer Oligo dT primer (5′ GCTGTCAACGATACGCTACGTAACGGCATGACAGTG$(T)_{18}$ 3′) was then used to prime first-strand cDNA synthesis by reverse transcription. The 5′ end of the 3′ cleaved fragment of the target transcript was amplified with the GeneRacer 5′ primer (5′ CGACTGGAGCACGAGGACACTGA 3′) and GeneRacer 5′ Nested Primer (5′ GGACACTGACATGGACTGAAGGAGTA 3′), and two nested target gene-specific primers (TGSPs) for two-round nested PCR amplification. The PCR products were gel-purified and cloned into pEASY-Blunt Cloning vector (TransGen Biotech, Beijing, China) for sequencing. The sequences of TGSPs are listed below:

AT1G48410-TGSP-1 (5′ AGCCTTGCTAGAAGAAGGTATAGG CTGG 3′)

AT1G48410-TGSP-2 (5′ CATCACAGCACGATTGACACCCCTT GATG 3′)

AT1G06580-TGSP-1 (5′ GCAAATCCTCCAGTCTCACCAATGC 3′)

AT1G06580-TGSP-2 (5′ GCTCATGCGCTTCACGCCATAGTC 3′)

AT1G62914-TGSP-1 (5′ GCTTAGCCTCACCAAGGCGATCGA GC 3′)

AT1G62914-TGSP-2 (5′ GTGACTACGTTTGGTAGACAATCCT TCC 3′)

AT3G27200-TGSP-1 (5′ TGGAAGCACGTAACCCATGACCTG 3′)

AT3G27200-TGSP-2 (5′ AGTGGAGTAGCGGTTGAGAAAACA TG 3′)

AT5G02350-TGSP-1 (5′ ACCGAGGCACACCGGAAGTCTATT TGGT 3′)

AT5G02350-TGSP-2 (5′ CTCGGAATGTGAGGAAATGTTTGTC GTGCT 3′)

AT1G19690-TGSP-1 (5′ TAACAAAGCCATCGAAGATTTCCA CTCG 3′)

AT1G19690-TGSP-2 (5′ CCATCCTTGTTCTGCAGCTAATCTC ACT 3′)

AT1G07990-TGSP-1 (5′ GTCGAAGAAATCCAGTGGACTCTC CATTTG 3′)

AT1G07990-TGSP-2 (5′ GTTCTCCCCACCCGACCCATTCG 3′)

3 | Results

3.1 | Identification of AGO1-Enriched sRNomes in Different Samples of *Arabidopsis*

To perform a comprehensive search for the sRNAs enriched in AGO1, the previously reported sRNA sequencing datasets prepared from the immunoprecipitated (IP) AGO1 protein of four different *Arabidopsis* samples, including flowers, leaves, roots, and seedlings (Wang et al. 2011), were retrieved for this study. To identify the AGO1-enriched sRNAs, the "three-fold" enrichment criterion was applied to make a relatively rigorous comparison between the "IP" dataset and the "input" dataset in each sample. Specifically, for an AGO1-enriched sRNA, its level (RPM) of the "IP" dataset should be higher than or equal to 3 times its level of "input." If the sRNA could not be detected in "input," its "IP" level should be higher than or equal to 1 RPM. As a result, a total of 42 991, 22 516, 34 555, and 19 754 sRNAs enriched in AGO1 were discovered from flowers, leaves, roots, and seedlings, respectively (Supporting Information Table S1). In *Arabidopsis*, selective sorting of sRNAs into the AGO complexes is largely determined by their 5′ terminal nucleotide composition and sequence length (Mi et al. 2008). Statistical results showed that more than 70% of the AGO1-enriched sRNAs started with U, and higher than 50% of these sRNAs were 21 or 22 nt in length in the three samples investigated, including flowers, leaves, and seedlings. However, an obvious difference was detected in roots that only 42.62% and 30.00% of the AGO1-enriched sRNAs identified from this organ started with U and were 21 or 22 nt in length, respectively (Figure 1A). The above observation indicates that the AGO1-enriched sRNome in roots is more heterogeneous than those identified from the other three samples. Since miRNAs and ta-siRNAs were two major classes known to be selectively incorporated into AGO1 (Fang and Qi 2016; Fei et al. 2013), we were curious whether the two sRNA classes were detectable in the AGO1-enriched sRNomes. To this end, 4803 mature miRNAs of the green plants (*Viridiplantae*) registered in miRBase (release 22) (Kozomara et al. 2019), including 428 registries of *Arabidopsis*, and 11 TAIR10-annotated *TAS* genes (Reiser et al. 2024) and two recently reported *TAS* candidate genes (Feng et al. 2024) were totally recruited as the references. The mapping results showed that 116 miRNAs of *Arabidopsis*, 101 miRNAs of the other green plants, and 1266 ta-siRNAs encoded by the *TAS* genes were detectable in the AGO1-enriched sRNome of flowers. In leaves, there are 84 miRNAs of *Arabidopsis*, 95 miRNAs of the other green plants, and 1572 ta-siRNAs detected from the AGO1-enriched sRNome. In roots, there are 51 miRNAs of *Arabidopsis*, 64 miRNAs of the other green plants, and 746 ta-siRNAs detected from the AGO1-enriched sRNome. In seedlings, there are 125 miRNAs of *Arabidopsis*, 103 miRNAs of the other green plants, and 2223 ta-siRNAs within the AGO1-enriched sRNome (Supporting Information Table S1). Summarily, a large portion of the *Arabidopsis* miRNAs and ta-siRNAs, which were well-documented in the AGO1-centered RNAi pathways (Fang and Qi 2016), were detectable in the four samples investigated. The result indicates that "three-fold" enrichment criterion is efficient for identification of the AGO1-enriched sRNAs. Additionally, the discovery of the miRNAs not reported in *Arabidopsis* but conserved in the other green plants points to the unsaturated *Arabidopsis* miRNA repository currently registered in miRBase (release 22).

13653040, 0, Downloaded from https://onlinelibrary.wiley.com/doi/10.1111/pce.70893 by Yijun Meng - Hangzhou Normal University , Wiley Online Library on [16/09/2026]. See the Terms and Conditions (https://onlinelibrary.wiley.com/terms-and-conditions) on Wiley Online Library for rules of use; OA articles are governed by the applicable Creative Commons License

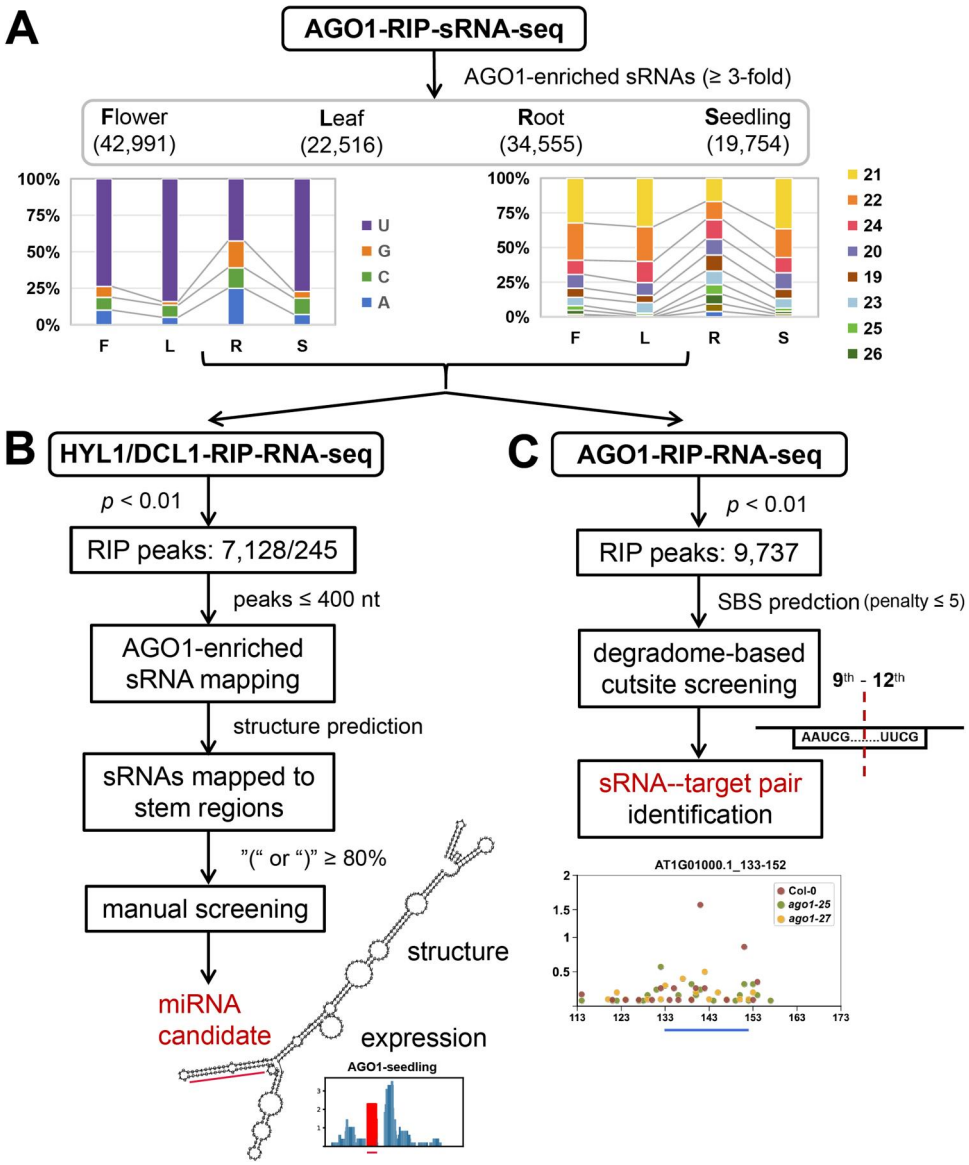


FIGURE 1 | Workflow of RIP-seq-based identification of the AGO1-enriched sRNome and targetome in *Arabidopsis*. (A) Identification of the AGO1-enriched sRNAs based on the AGO1-RIP-sRNA-seq data. The sequencing datasets of four samples (F: flowers; L: leaves; R: roots; and S: seedlings) enabled us to identify the AGO1-enriched sRNAs (≥ 3 folds enrichment) through an organ-specific manner. The 5′ nucleotide composition and the sequence length distribution were analyzed for the four sRNA groups, respectively. (B) Identification of the microRNA candidates based on the RIP-RNA-seq data of HYL1 and DCL1. (C) Identification of the targets regulated by the AGO1-enriched sRNAs by integrated analysis of the AGO1-RIP-RNA-seq data and the degradome-seq data. [Color figure can be viewed at wileyonlinelibrary.com]

3.2 | Identification of miRNA Candidates Based on the RIP-RNA-Seq Data of DCL1 and HYL1, and Structure Prediction

The discovery above showed that more than 100 mature miRNA candidates had not been reported for *Arabidopsis*, but were present in the other green plants. Based on the evolutionary model, the canonical miRNAs are gradually evolved from the young miRNAs whose expression levels are relatively low and precursor structures are not well-organized (Cuperus et al. 2011). In this regard, we set out to perform a tentative search for the miRNA candidates from the AGO1-enriched sRNomes of the four different samples.

Considering the fact that DCL1 was an indispensible factor for miRNA processing through direct binding onto the miRNA precursors, the recently reported RNA-seq dataset of the immunoprecipitated DCL1 protein (Bologna et al. 2026) was used for miRNA precursor identification. Since HYL1 was another key factor for miRNA maturation, two biological replicates of the RNA-seq experiment of the immunoprecipitated HYL1 protein were performed in the present study. The IP result showed that the HYL1 protein (~68 kDa) was detectable in both "input" and "IP" samples, and the signals were especially stronger in the "IP" samples. But for "IgG control," HYL1 could be hardly detected, indicating the specificity of our IP experiments for HYL1-RIP-seq (Supporting Information Figure S1). Based on the RIP-RNA-seq data, 245 and 7128 RIP peaks of DCL1 (Bologna et al. 2026) and HYL1 (Supporting Information Table S2), representing the transcriptome-wide binding regions of the two proteins, respectively, were obtained for further

13653040, 0, Downloaded from https://onlinelibrary.wiley.com/doi/10.1111/pce.70893 by Yijun Meng - Hangzhou Normal University , Wiley Online Library on [16/09/2026]. See the Terms and Conditions (https://onlinelibrary.wiley.com/terms-and-conditions) on Wiley Online Library for rules of use; OA articles are governed by the applicable Creative Commons License

analyses. Next, we were interested in the association between the RIP peaks and the already annotated miRNA precursors. In plants, the primary microRNAs (pri-miRNAs) are usually unstable, and their full-length sequences are difficult to be cloned. Thus, most of the precursors registered in miRBase are the secondary precursors called precursor microRNAs (pre-miRNAs). In this regard, both upstream and downstream regions were extended to 500 nt in length for each of the 326 miRBase-registered (release 22) miRNA precursors of *Arabidopsis*. It was observed that a total of 72 extended miRNA precursors overlapped with the HYL1 RIP peaks. Notably, among these, 34 precursors could be simultaneously detected by the two replicates (Supporting Information Table S3). However, possibly due to the small volume of the DCL1 RIP data, none of the miRNA precursors were observed to overlap with the RIP peaks of DCL1. Anyway, the result above supports the notion that miRNA precursors are bound by HYL1 for two-step processing, and at least a part of the precursors, including novel candidates can be detected by RIP-RNA-seq of HYL1.

In order to identify the miRNA precursor candidates, we first mapped the 42 991, 22 516, 34 555, and 19 754 AGO1-enriched sRNAs discovered from flowers, leaves, roots, and seedlings to the RIP peak regions, respectively. Then, those regions containing the perfectly mapped AGO1-enriched sRNAs were sent to RNAfold (Lorenz et al. 2011) for secondary structure prediction. Based on the predictions, we focused on the sRNA-coding loci resided within the "stem" structures (i.e., with ≥ 80% base-paired regions) (Figure 1B). Finally, manual screening was performed to extract the relatively reliable precursor candidates based on: (1) the "stem" regions encoding the AGO1-enriched sRNAs should be encompassed by the hairpin-like structures; and (2) the expression levels of the sRNAs encoded by the "stem" regions should be obviously higher than those mapped to the other regions of the precursors. As a result, seven and seven precursor candidates were identified from the RIP peaks of HYL1 and DCL1, respectively (Figure 2 and Supporting Information Figure S2). Detailed investigation revealed that some of the "stem" regions encoding the AGO1-enriched sRNAs were allocated to the hairpin-like substructures (Figure 2A,B), while some were resided within the main hairpin structures (Figure 2C–F). Additionally, it was observed that some of the mature miRNA candidates were consistently expressed in different organs (the sRNA IDs highlighted in green in Figure 2A,E), while some were organ-specifically expressed (Figure 2B–D,F). Another interesting phenomenon was observed that some precursors harbored

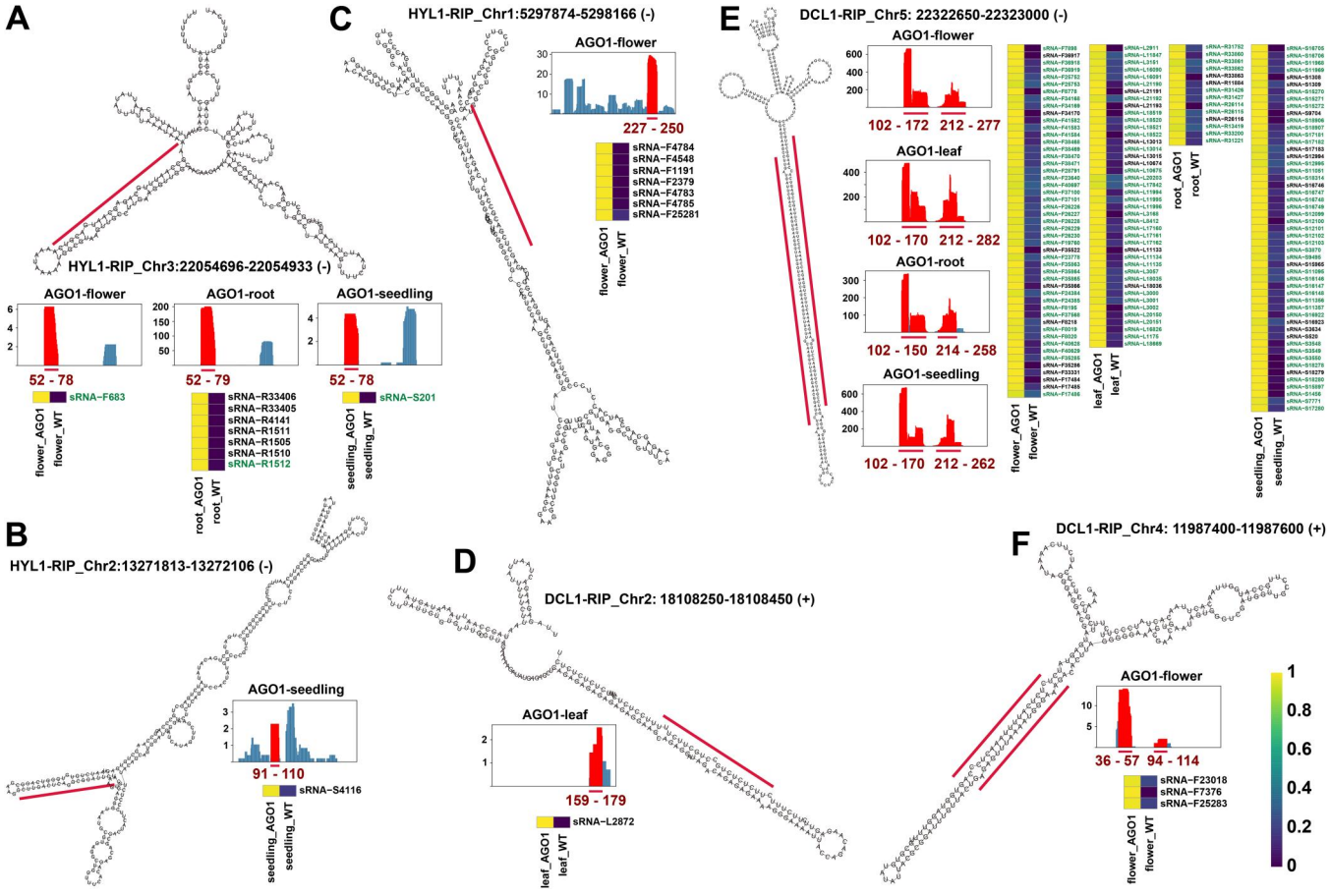


FIGURE 2 | Examples of the microRNA (miRNA) candidates identified based on the RIP-RNA-seq data of HYL1 (A–C) and DCL1 (D–F). For all of the candidates, the RIP peak sequences were used to predict the secondary structures of the miRNA precursors. And, the stem regions encoding the mature miRNAs were marked by red lines. Based on the AGO1-RIP-sRNA-seq data, the sRNA expression patterns all along the miRNA precursors were shown by histograms (*x* axes indicating the positions on the precursors; *y* axes measuring the sRNA expression levels in RPM, reads per million). The heatmaps show the evidence of the AGO1 enrichment for the mature miRNA candidates. [Color figure can be viewed at wileyonlinelibrary.com]

13653040, 0, Downloaded from https://onlinelibrary.wiley.com/doi/10.1111/pce.70893 by Yijun Meng - Hangzhou Normal University , Wiley Online Library on [16/09/2026]. See the Terms and Conditions (https://onlinelibrary.wiley.com/terms-and-conditions) on Wiley Online Library for rules of use; OA articles are governed by the applicable Creative Commons License

the long "stem" regions producing the AGO1-enriched sRNAs (Figure 2C–F and Supporting Information Figure S2). For an extreme case, a precursor candidate detected from the RIP-seq data of DCL1 harbored a 100-bp-long "stem," within which a continuously paired 60-bp region was observed to be a hotspot for sRNA production. On this region, the expression patterns of the AGO1-enriched sRNAs were highly consistent in all of the four samples investigated (Figure 2E).

3.3 | AGO1-RIP-RNA-Seq-Based Target Identification, and Degradome-Based AGO1 Dependency Analysis

In plants, the AGO1-enriched sRNAs, such as miRNAs, ta-siRNAs, vsiRNAs, and possibly some unknown species, can guide the RISC complexes to the complementary SBSs for target cleavage (Fang and Qi 2016; Fei et al. 2013; Jones-Rhoades et al. 2006; Yu et al. 2026). In the present study, the direct interaction between target transcripts and the AGO1-centered RISCs became the key basis for discovering the novel targets regulated by the AGO1-enriched sRNAs by analyzing the RIP-RNA-seq data of AGO1. Two biological replicates of the AGO1-RIP-RNA-seq experiment were performed. The IP result showed that the AGO1 protein (~130 kDa) was detectable in both "input" and "IP" samples, and the signals were especially stronger in the "IP" samples. But for "IgG control," AGO1 could be hardly detected, indicating the specificity of our IP experiments for AGO1-RIP-seq (Supporting Information Figure S1). As a result, a total of 9737 RIP peaks assigned to 6463 genes were detected, which represented the transcriptome-wide binding regions of the AGO1 protein (Supporting Information Table S2). Next, all of these RIP peaks were submitted to TargetFinder (penalty ≤ 5) (Fahlgren and Carrington 2010), in order to predict the SBSs of the AGO1-enriched sRNAs identified seedlings (Figure 1C). Theoretically, the RIP-RNA-seq data of AGO1 provided another layer to reduce the false positive rate of the SBS predictions.

Degradome-seq is an experimental tool for high-throughput mapping of the slicing sites in the middle of the predicted SBSs (Y. Meng et al. 2011). In this regard, we set out to perform degradome-seq experiments for the seedlings of *Arabidopsis*, in order to validate the predicted SBSs resided within the RIP peaks of AGO1. First, the degradome-seq dataset of the WT seedlings of Col-0 was utilized to validate the SBSs predicted for the AGO1-enriched sRNAs of seedlings, according to the previously reported method (Shao et al. 2013) (Figure 1C). As a result, a total of 456 pairs involving 453 AGO1-enriched sRNAs and 44 target genes were verified by the degradome signatures in WT (Supporting Information Table S4). Since the present study was based on the direct association of AGO1 with both sRNAs and the target transcripts, we were curious about the AGO1 dependency of the 456 sRNA–target pairs. In this regard, degradome-seq was also performed for the two *ago1* mutants, *ago1-25* and *ago1-27*. Degradome data analysis showed that 153 out of the 456 pairs were validated in *ago1-25*, only 13 pairs were validated in *ago1-27*, and six pairs were validated in both mutants (Supporting Information Table S4).

According to the previous report, although *ago1-25* and *ago1-27* carry missense mutations, both mutants can express the mutated AGO1 proteins, and no significant difference of the AGO1 protein levels were detected between the two mutants (Sánchez-García et al. 2015). The partially impaired AGO1 activity may explain why some of the targets detected in WT could also be detected in the two hypomorphic mutants (Figure 3A). On the other hand, the AGO1 protein levels cannot explain the discrepancy observed between the two *ago1* mutants in the present study. It is worth noting that *ago1-27* was reported to be more responsive to environmental perturbations compared with *ago1-25* (Stief et al. 2014; Mason et al. 2016), which may partially explain the difference between the two *ago1* mutants observed in the present study. The detailed molecular mechanisms underlying the remarkable discrepancy between the two *ago1* mutants need further investigations. Anyway, the more important point was that the remaining 284 pairs (62.28% out of the total pairs) not validated in the two mutants were specifically detected in WT (Figure 3A). Taken together, the results showed that a large portion of the sRNA–target pairs discovered in WT could not be detected in the *ago1* mutants, especially in *ago1-27*, demonstrating the AGO1 dependency of the sRNA target sites discovered from the AGO1-RIP-RNA-seq data. In other words, the results support the feasibility of our AGO1-RIP-based workflow (Figure 1C).

Further analysis was performed for the 456 sRNA–target pairs validated in the WT plants. First, a comparison of the distribution patterns between the validated SBSs and the AGO1 RIP peaks covering these SBSs was performed. Notably, their distribution patterns on the target transcripts were quite similar that a prominent enrichment was allocated to the 3′ ends of the CDS (coding sequence) regions, and a small but significant enrichment was also detected between 5′UTR and the 5′ ends of the CDSs (the left panel of Figure 3B). Moreover, GO term enrichment analysis of the 44 target genes belonging to the 456 regulatory pairs showed that a significant portion of these genes were functionally related to transcriptional regulation (the right panel of Figure 3B). Finally, some of the sRNA–target pairs were taken as an example for graphic illustrations (Figure 3C–E and Supporting Information Figure S3). For the first case, the AGO1 RIP peak covering the validated SBS was detected on the first exon of *AT1G48410* encoding the AGO1 protein itself (Figure 3C). One of the AGO1-enriched sRNAs identical to ath-miR168b-5p registered in miRBase (release 22) was identified as the regulator of *AT1G48410*, supporting the feedback regulation of *AGO1* by the miRNA pathway reported by a previous study (Vaucheret et al. 2004). It was also noticed that in addition to ath-miR168b-5p, another 11 sRNAs enriched in AGO1 were also identified to be the potential regulators of *AGO1*, since these sRNAs targeted to the identical SBS based on high sequence complementarity. In seedlings, expression pattern analysis showed that all of the 12 above mentioned sRNAs were highly enriched in the AGO1-IP sample compared to the input sample (the left heatmap of Figure 3C). Besides, the levels of these sRNAs were deeply reduced in the two *ago1* mutants (the right heatmap of Figure 3C), pointing to the influence of the *ago1* mutation not only on the endonuclease activity of the AGO1 protein itself, but also on the abundance of the AGO1-enriched sRNAs. The target plot (t-plot) presenting the degradome mapping result showed clearly that the specific cleavage signal in the middle of the SBS was detectable in WT but not in the mutants (Figure 3C). For another two cases, the

13653040, 0, Downloaded from https://onlinelibrary.wiley.com/doi/10.1111/pce.70893 by Yijun Meng - Hangzhou Normal University , Wiley Online Library on [16/09/2026]. See the Terms and Conditions (https://onlinelibrary.wiley.com/terms-and-conditions) on Wiley Online Library for rules of use; OA articles are governed by the applicable Creative Commons License

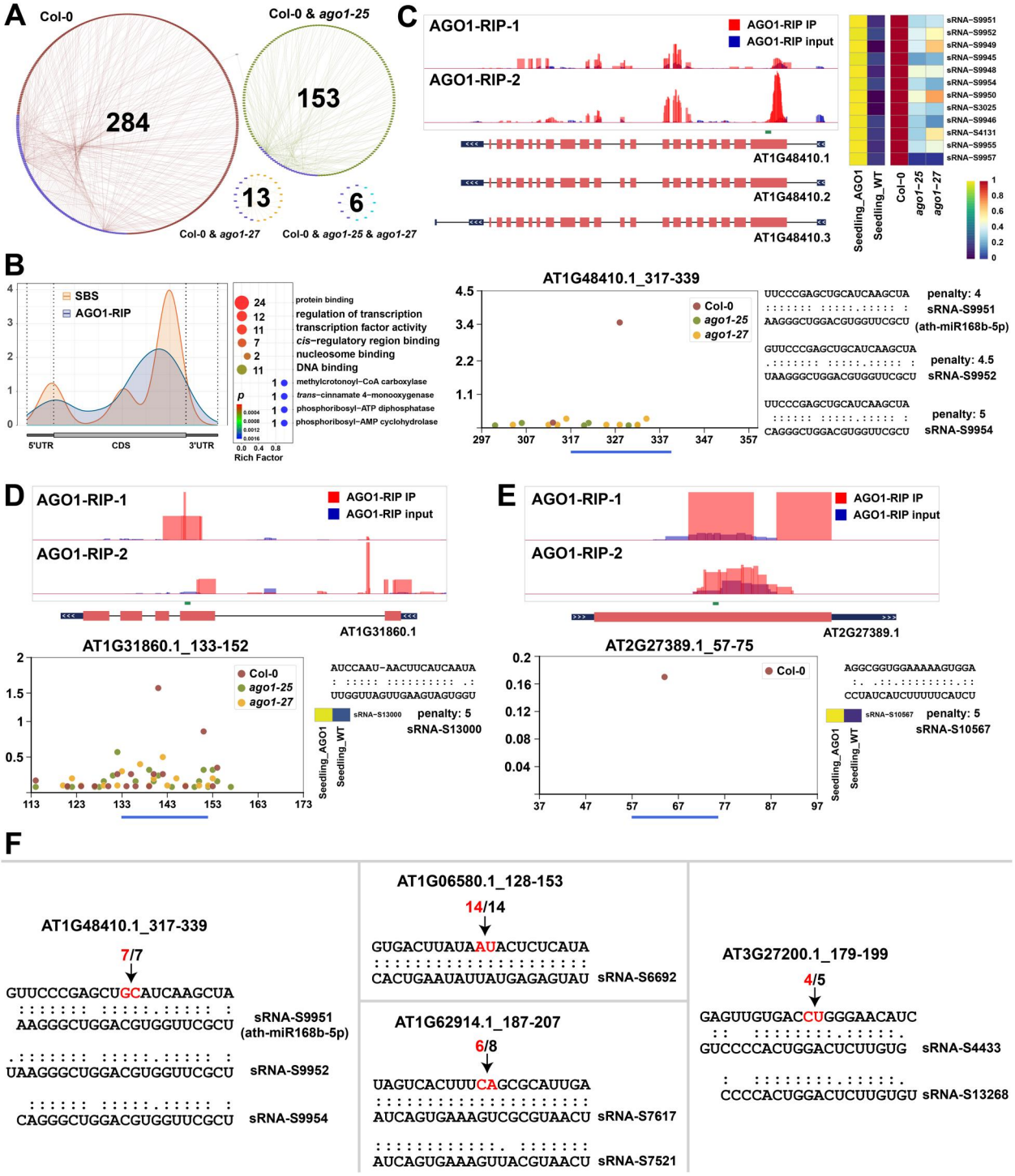


FIGURE 3 | Identification of the targets regulated by the AGO1-enriched sRNAs in the seedlings of wild-type plants and the two *ago1* mutants (*ago1-25* and *ago1-27*). (A) Networks showing the degradome-supported sRNA–target pairs identified from the wild-type plants (Col-0), *ago1-25*, and *ago1-27*, respectively. A total of 284 pairs were specifically identified from Col-0, 153 pairs could be identified in both Col-0 and *ago1-25*, 13 pairs could be identified in both Col-0 and *ago1-27*, and six pairs were identified in all of the three samples. (B) In-depth analysis of all sRNA–target pairs identified from Col-0. Left panel: metagene profile showing the distribution patterns of the degradome-supported SBSs and the AGO1 RIP peaks covering these SBSs. Right panel: GO (Gene Ontology) term enrichment analysis of the taget genes. (C–E) Examples showing the AGO1-dependent sRNA–target pairs identified from Col-0. For each case, the IGV (Integrative Genomics Viewer) window shows the AGO1 binding signals on the target transcript based on the AGO1-RIP-RNA-seq data (the SBS was indicated by a short green bar). The target plot (t-plot) presenting the degradome signatures mapped onto the target transcript provides the evidence of sRNA-guided cleavage (*x* axes indicating the positions on the target transcripts; *y* axes measuring the levels of the degradome signals in RPM, reads per million). The heatmap shows the evidence of the AGO1 enrichment for the regulatory sRNA(s). (F) Validation of the SBSs on four target genes (*AT1G48410*, *AT1G06580*, *AT1G62914*, and *AT3G27200*) by modified 5′RACE. For each SBS, the validated slicing site was marked by an arrow with the numbers showing the number of the total sequenced clones and the number of the sequenced clones supporting the slicing site. [Color figure can be viewed at wileyonlinelibrary.com]

13653040, 0, Downloaded from https://onlinelibrary.wiley.com/doi/10.1111/pce.70893 by Yijun Meng - Hangzhou Normal University , Wiley Online Library on [16/09/2026]. See the Terms and Conditions (https://onlinelibrary.wiley.com/terms-and-conditions) on Wiley Online Library for rules of use; OA articles are governed by the applicable Creative Commons License

AGO1 RIP peaks covering the validated SBSs of two AGO1-enriched sRNAs were detected on the exonic regions of *AT1G31860* and *AT2G27389*, respectively. In both cases, prominent degradome signals from the WT seedlings but not from the *ago1* mutants were detected in the middle of the SBSs (Figure 3D,E). Notably, although enriched in AGO1, the two sRNA regulators are neither the miRBase-registered miRNAs nor the ta-siRNAs, indicating the involvement of the other sRNA species in guiding the AGO1 complexes for target cleavage. To further examine the reliability of the target sites validated by degradome-seq data, a total of five SBSs shown in Figure 3 and Supporting Information Figure S3 were randomly selected for slicing site mapping by employing modified 5′RACE (rapid amplification of cDNA ends). As a result, four SBSs on the target genes *AT1G48410*, *AT1G06580*, *AT1G62914*, and *AT3G27200* were verified (Figure 3F and Supporting Information Figure S4), pointing to the reliability of the targetomes discovered based on our workflow.

3.4 | Identification of the Ecotype-Specific Targetomes

The feasibility of the AGO1-RIP-RNA-seq-based identification of the sRNA-regulated targetome was verified in the above analysis. Next, we would like to examine the utility of this method in different scenarios. It is well-known that the plant sRNAs play critical regulatory roles in diverse biological processes related to development, reproduction and stress response (X. M. Chen 2009). In this regard, the distinct environmental adaptability exhibited by different ecotypes of *Arabidopsis* might be partially attributed to the differential sRNA–target regulation. Thus, for the first attempt, we set out to analyze the degradome-seq data from the seedlings of the seven *Arabidopsis* ecotypes (Altai-5, Col-0, ICE73, Kas-2, Kondara, Se-0, and Zal-1) reported by a recent study (Feng et al. 2026), in order to interrogate the differentiated sRNA targetomes in these ecotypes. Based on degradome mapping, validation of the AGO1 RIP peak-covered SBSs predicted for the AGO1-enriched sRNAs of seedlings was performed for the seven ecotypes, respectively. We focused on the ecotype-specific sRNA–target pairs supported by clear degradome evidence. As a result, 62 pairs involving 62 sRNAs and 29 target genes, 86 pairs involving 86 sRNAs and 42 genes, 101 pairs involving 100 sRNAs and 43 genes, 68 pairs involving 64 sRNAs and 33 genes, 72 pairs involving 72 sRNAs and 33 genes, 58 pairs involving 57 sRNAs and 27 genes, and 71 pairs involving 70 sRNAs and 37 genes, were specifically detected in Altai-5, Col-0, ICE73, Kas-2, Kondara, Se-0, and Zal-1, respectively (Figure 4A and Supporting Information Table S5). To further examine the reliability of the ecotype-specific sRNA–target pairs identified above, four pairs were randomly selected for slicing site mapping by using modified 5′RACE. As a result, three SBSs on the target genes *AT5G02350*, *AT1G19690*, and *AT1G07990* were verified (Supporting Information Figure S5), pointing to the reliability of these ecotype-specific targetomes. For the ecotype-specific targetomes, the metagene profiles showed that the distribution patterns of the validated SBSs were to some extent similar to those of the AGO1 RIP peaks covering these SBSs (Figure 4B–H). However, the distribution patterns were distinguishable among different ecotypes. For example, in Col-0, Kas-2, and Zal-1, a prominent enrichment was allocated to the 3′ ends of the CDSs, and a small enrichment was also detected between 5′UTR and the 5′ ends of the CDSs. In ICE73 and Kondara, the prominent enrichment was detected at both ends of the CDSs. It was reported that the seven ecotypes analyzed above were originated from the natural habitats with quite different environmental parameters involving precipitation, temperature, and solar radiation (Feng et al. 2026). In this regard, it was interesting to investigate the biological functions of the ecotype-specific targetomes. GO term enrichment analysis (hypergeometric test, $p < 0.01$; the top 10 GO terms were selected) of these targetomes uncovered certain notable functional hints related to environmental response or development. Specifically, for the Col-0-specific targetome, the genes are functionally enriched in "response to osmotic stress" and "response to water deprivation" (Figure 4B). Intriguingly, compared to the other six ecotypes, the annual precipitation of the natural habitat of Col-0 is especially high (Feng et al. 2026). In Altai-5, the targetome is functionally enriched in "leaf patterning" (Figure 4C). In ICE73, the targetome is functionally enriched in "pollen acceptance" (Figure 4D). In Kas-2, the targetome is functionally enriched in "leaf patterning" and "adventitious root development" (Figure 4E). And, in Se-0, its specific targetome is functionally enriched in "respiratory burst" and "root development" (Figure 4G). The observed functional hints indicate that the phenotypic and physiological features involving organ development, reproduction, and environmental adaptability, which are distinguishable among different ecotypes, might be partially attributed to the ecotype-specific targetomes.

According to the *Arabidopsis* 1001 Genomes Project (1001-Alonso-Blanco et al. 2016), huge amounts of SNPs (single nucleotide polymorphisms) exist in distinct *Arabidopsis* ecotypes. Thus, we were curious about the influence of the SNPs on sRNA–target interactions in the six ecotypes. We focused on the ecotype-specific sRNA–target pairs containing SNPs within the SBS sequences. And, the penalty scores of these SNP-interfered pairs were recalculated by TargetFinder, in order to reevaluate the altered affinity of the sRNA–target interactions. As a result, among the 86 Col-0-specific sRNA–target pairs, 14 pairs were observed to contain SNPs within the SBS sequences. Notably, compared to Col-0, the interaction affinity of 12 pairs was suggested to be reduced in some of the other six ecotypes based on the increased penalty scores induced by the SNPs (Supporting Information Table S5). A total of nine Altai-5-specific sRNA–target pairs were identified to have SNPs within the SBS sequences. Notably, compared to Col-0, the binding affinity of two pairs was suggested to be elevated considering the down-regulated penalty scores in Altai-5. And, the binding affinity of another five pairs was likely to be reduced in some of the remaining five ecotypes (ICE73, Kas-2, Kondara, Se-0, and Zal-1), considering the up-regulated penalty scores in these ecotypes (Supporting Information Table S5). A total of nine ICE73-specific sRNA–target pairs were identified to have SNPs within the SBS sequences. Notably, compared to Col-0, the binding affinity of seven pairs was possibly reduced in some of the remaining five ecotypes (Altai-5, Kas-2, Kondara, Se-0, and Zal-1), based on the up-regulated penalty scores in these ecotypes (Supporting Information Table S5). Five Kas-2-specific sRNA–target pairs were discovered to have SNPs within the

13653040, 0, Downloaded from https://onlinelibrary.wiley.com/doi/10.1111/pce.70893 by Yijun Meng - Hangzhou Normal University , Wiley Online Library on [16/09/2026]. See the Terms and Conditions (https://onlinelibrary.wiley.com/terms-and-conditions) on Wiley Online Library for rules of use; OA articles are governed by the applicable Creative Commons License

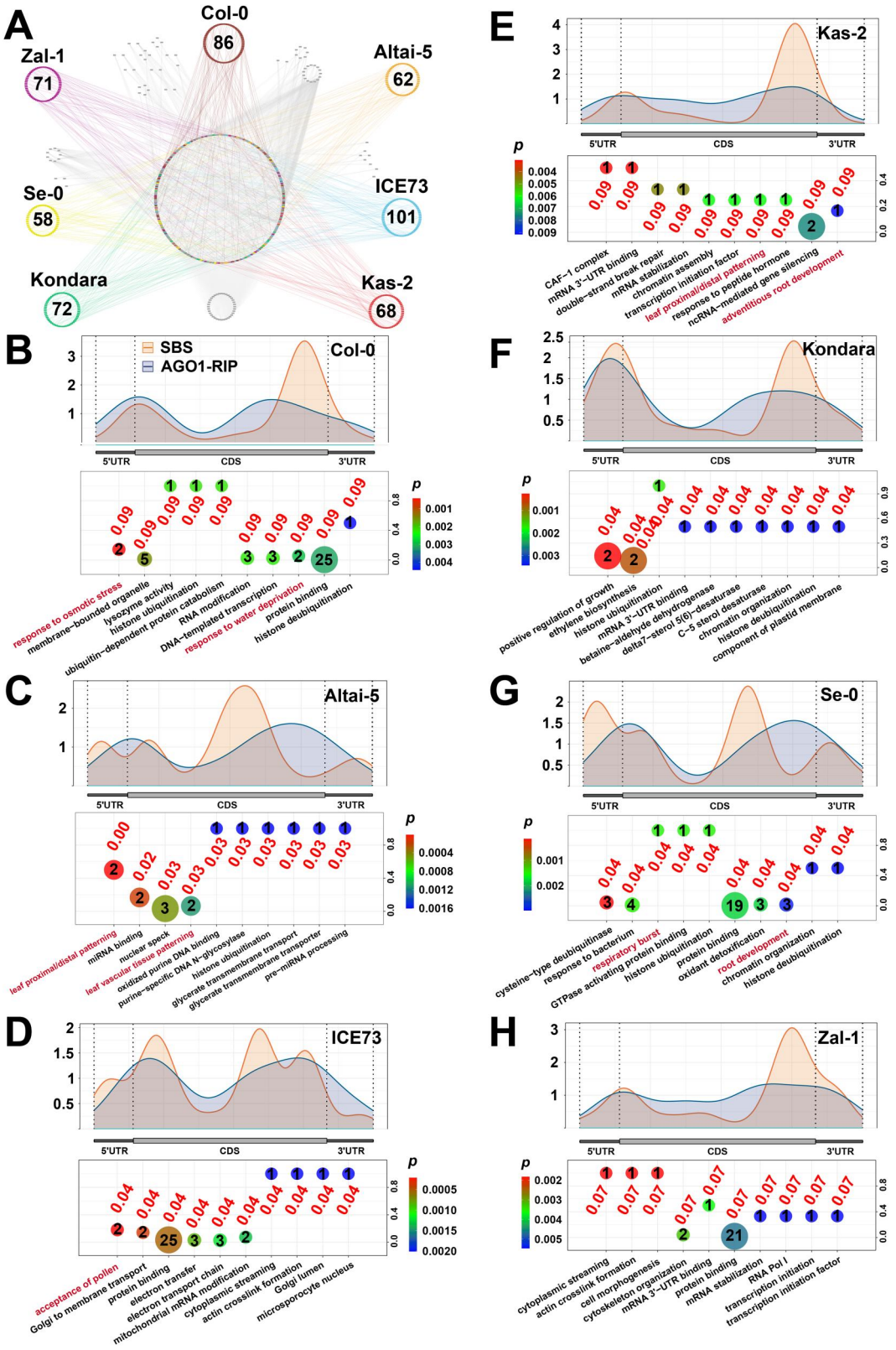


FIGURE 4 | Identification and characterization of the ecotype-specific targetomes. (A) Networks showing the degradome-supported sRNA–target pairs specifically identified from one of the seven ecotypes analyzed. A total of 86, 62, 101, 68, 72, 58, and 71 ecotype-specific pairs were identified from Col-0, Altai-5, ICE73, Kas-2, Kondara, Se-0, and Zal-1, respectively. (B–H) In-depth analysis of the ecotype-specific sRNA–target pairs. Upper panels: metagene profiles showing the distribution patterns of the degradome-supported SBSs and the AGO1 RIP peaks covering these SBSs. Lower panel: GO (Gene Ontology) term enrichment analyses (hypergeometric test, $p < 0.01$; the top 10 GO terms were selected) of the taget genes (the GO terms related to environmental response or development were highlighted in red). For each GO term, the Q values (< 0.1) calculated by the Benjamini–Hochberg procedure is also shown (in red) adjacent to the bubble for reference. [Color figure can be viewed at wileyonlinelibrary.com]

13653040, 0, Downloaded from https://onlinelibrary.wiley.com/doi/10.1111/pce.70893 by Yijun Meng - Hangzhou Normal University , Wiley Online Library on [16/09/2026]. See the Terms and Conditions (https://onlinelibrary.wiley.com/terms-and-conditions) on Wiley Online Library for rules of use; OA articles are governed by the applicable Creative Commons License

SBSs. Compared to Col-0, the binding affinity of these pairs was likely to be reduced in Altai-5, ICE73, and/or Se-0, considering the increased penalty scores in these ecotypes (Supporting Information Table S5). Eight Kondara-specific pairs were discovered to have SNPs within the SBSs. Compared to Col-0, the binding affinity of the eight pairs was likely to be reduced in Altai-5, Kas-2, Se-0, and/or Zal-1, based on the increased penalty scores in these ecotypes (Supporting Information Table S5). Taken together, the observations above indicate that genomic variations may influence sRNA–target interactions in specific ecotypes, resulting in ecotype-specific targetomes.

3.5 | Identification of the Organ- and Temperature-Specific Targetomes

The above study showed that integrated analysis of the AGO1-RIP-RNA-seq data and the degradome-seq data enabled us to efficiently identify the ecotype-specific targetomes. The previously reported degradome datasets of four different samples under three different temperature treatments (Gyula et al. 2018) evoked our interesting in identification of the organ- and temperature-specific targetomes in *Arabidopsis*. To this end, the 9737 AGO1 RIP peaks were submitted to TargetFinder (penalty ≤ 5) (Fahlgren and Carrington 2010), in order to predict the binding sites of the AGO1-enriched sRNAs of flowers, leaves, roots, and seedlings, respectively. Then, the reported degradome datasets of 12 samples (flowers, leaves, roots, and seedlings under 15°C, 21°C, and 27°C, respectively) with two biological replicates were used to map the slicing sites within the SBSs predicted above.

A comparison among the targetomes validated by the degradome data of the four samples under the same temperature enabled us to identify the organ-specific targetomes. Specifically, 183 flower-specific pairs involving 181 sRNAs and 101 target genes, 133 leaf-specific pairs involving 130 sRNAs and 68 genes, 299 root-specific pairs involving 294 sRNAs and 91 genes, and 353 seedling-specific pairs involving 339 sRNAs and 90 genes were identified under the 15°C treatment. A total of 297 flower-specific pairs involving 293 sRNAs and 140 genes, 214 leaf-specific pairs involving 206 sRNAs and 100 genes, 375 root-specific pairs involving 341 sRNAs and 93 genes, and 247 seedling-specific pairs involving 229 sRNAs and 106 genes were identified under 21°C. A total of flower-specific 283 pairs involving 275 sRNAs and 143 genes, 284 leaf-specific pairs involving 281 sRNAs and 96 genes, 341 root-specific pairs involving 303 sRNAs and 98 genes, and 215 seedling-specific pairs involving 196 sRNAs and 93 genes were identified under 27°C (Figure 5A and Supporting Information Table S6). All of the targetomes identified under different temperature treatments were classified into four groups: flower-specific, leaf-specific, root-specific, and seedling-specific ones. Then, the gene set belonging to each group was sent for GO term enrichment analysis (hypergeometric test, $p < 0.01$; the top 10 GO terms were selected). As a result, the flower-specific targetome was functionally enriched in "flower development" and "transmitting tissue development," the leaf-specific targetome was functionally related to "chloroplast thylakoid membrane" and "embryo development ending," the root-specific targetome was functionally involved in "adventitious root development," and the seedling-specific targetome was functionally enriched in "cell differentiation" (Figure 5C). Notably, in many cases, the enriched GO terms are tightly linked to the organ specificity of each targetome. Based on the degradome-validated sRNA–target pairs, we also tried to identify the temperature-specific targetomes in each organ. As a result, 143 15°C-specific pairs involving 141 sRNAs and 86 genes, 239 21°C-specific pairs involving 235 sRNAs and 130 genes, and 256 27°C-specific pairs involving 249 sRNAs and 125 genes were identified in flowers. In leaves, 101 15°C-specific pairs involving 100 sRNAs and 56 genes, 164 21°C-specific pairs involving 160 sRNAs and 85 genes, and 273 27°C-specific pairs involving 272 sRNAs and 83 genes were identified. In roots, 233 15°C-specific pairs involving 231 sRNAs and 76 genes, 250 21°C-specific pairs involving 230 sRNAs and 72 genes, and 243 27°C-specific pairs involving 228 sRNAs and 84 genes were identified. In seedlings, 483 15°C-specific pairs involving 477 sRNAs and 83 genes, 216 21°C-specific pairs involving 204 sRNAs and 92 genes, and 198 27°C-specific pairs involving 179 sRNAs and 83 genes were identified (Figure 5B and Supporting Information Table S7). Different from the organ-specific targetomes, the enriched GO terms of the temperature-specific targetomes are not clearly linked to the temperature sensitivity (Figure 5C). Moreover, for all of the sRNA–target pairs identified from distinct organs under different temperature treatments, the metagene profiles showed that the distribution patterns of the validated SBSs were similar to those of the AGO RIP peaks covering these SBSs (Figure 5C).

3.6 | Identification of the lncRNAs Targeted by the AGO1-Enriched sRNAs

In the above analyses, we noticed that most of the AGO1 RIP peaks containing the degradome-validated SBSs were overlapped with the TAIR10-annotated protein-coding genes, while the remaining peaks were not. It would be interesting to investigate whether these unannotated peaks were originated from the lncRNAs, since most of the plant lncRNAs were transcribed by RNA polymerase II (Wierzbicki et al. 2021), and could also be included in the AGO1-RIP-RNA-seq libraries. To this end, we set out to identify the overlaps between the unannotated peaks and the *Arabidopsis* lncRNAs retrieved from CANTATAdb 3.0 (Szcześniak and Wanowska 2024) and PscLncRNA (Xu et al. 2025). As a result, 10 AGO1 RIP peaks containing the degradome-validated SBSs were reannotated with 11 lncRNAs, resulting in a total of 50 sRNA–target pairs involving 38 regulatory sRNAs (Supporting Information Table S8). Some of these pairs were used for graphic presentation (Figure 6 and Supporting Information Figure S6). Specifically, an intronless lncRNA (CNT30375214) overlapped with an AGO1 RIP peak was regulated by an AGO1-enriched sRNA identified from seedlings. Notably, the sRNA was fully complementary to the lncRNA, and the cleavage signal in the middle of the SBS was specifically detected in the WT seedlings of Col-0 (Figure 6A). Another case with four fully complementary SBSs was discovered for an intron-containing lncRNA (CNT30375369). In the middle of each SBS, a prominent cleavage signal was detected by degradome-seq. But notably, the slicing signatures of different SBSs showed distinct sample specificity, including roots under 27°C, seedlings under 21°C,

13653040, 0, Downloaded from https://onlinelibrary.wiley.com/doi/10.1111/pce.70893 by Yijun Meng - Hangzhou Normal University , Wiley Online Library on [16/09/2026]. See the Terms and Conditions (https://onlinelibrary.wiley.com/terms-and-conditions) on Wiley Online Library for rules of use; OA articles are governed by the applicable Creative Commons License

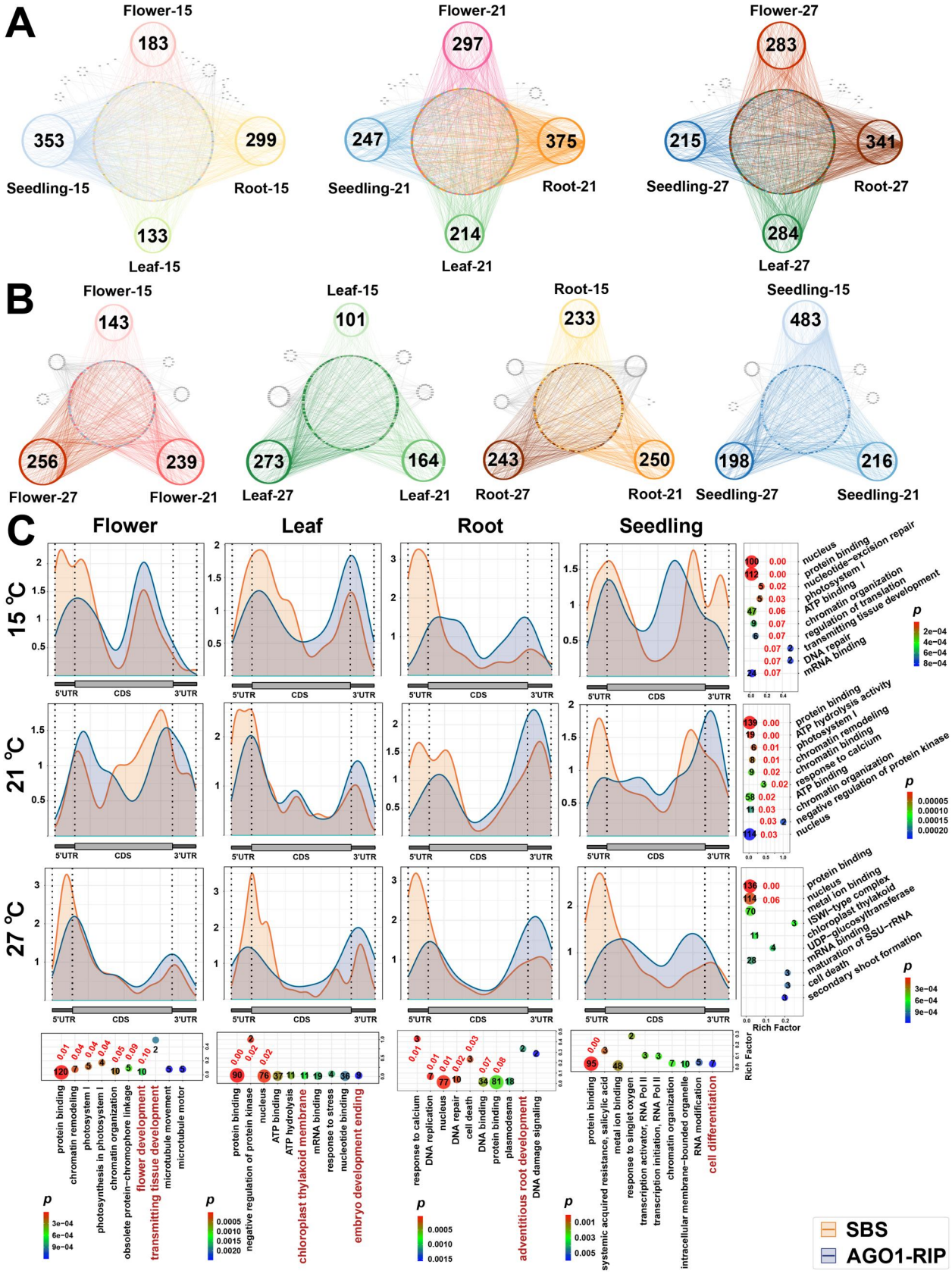


FIGURE 5 | Legend on next page.

13653040, 0, Downloaded from https://onlinelibrary.wiley.com/doi/10.1111/pce.70893 by Yijun Meng - Hangzhou Normal University , Wiley Online Library on [16/09/2026]. See the Terms and Conditions (https://onlinelibrary.wiley.com/terms-and-conditions) on Wiley Online Library for rules of use; OA articles are governed by the applicable Creative Commons License

Altai-5, and Kondara, respectively (Figure 6B). It indicated that post-transcriptional regulation of CNT30375369 by the AGO1-enriched sRNAs might be performed at different SBSs in distinct samples of *Arabidopsis*. Another two cases showing the organ- and temperature-specific regulation were described here. Two lncRNAs, ATHNATLNC001773 and CNT30371716, were regulated by the AGO1-enriched sRNAs, which were specifically supported by the degradome libraries prepared from the flowers under 15°C and the roots under 21°C, respectively (Figure 6C,D). Notably, in both cases, the SBSs are allocated to the intronic regions of the lncRNAs, pointing to the regulatory effect on these non-coding transcripts before their maturation. Some other organ-, temperature-, or ecotype-specific cases were provided in Supporting Information Figure S6. However, in some cases, the sRNA-mediated regulation showed relatively low specificity. For example, based on the degradome data, the lncRNA CNT30372447 was regulated by the AGO1-enriched sRNAs identified from flowers and seedlings (Figure 6E). Taken together, our results show that the AGO1-enriched sRNAs can not only target to the protein-coding genes, but also to the lncRNAs, and in many cases, this kind of post-transcriptional regulation is organ-, temperature-, or ecotype-specific.

4 | Discussion

In the present study, we showed the utility of RIP-seq data for plant sRNA studies. First, AGO1-RIP-sRNA-seq enabled us to identify the AGO1-enriched sRNomes from different organs of *Arabidopsis*. It is well known that nearly all of the mature miRNAs are selectively incorporated into the AGO1-centered silencing complexes in *Arabidopsis*. Thus, it was be interesting whether novel miRNA candidates could be identified from the AGO1-enriched sRNomes. On the other hand, HYL1 and DCL1 are two key players in processing the mature miRNAs from their precursors (Jones-Rhoades et al. 2006; Yu et al. 2026). In this regard, integrated analysis of the AGO1-enriched sRNomes and the RIP-RNA-seq data of HYL1 and DCL1 promoted us to identify novel miRNA precursors (Figure 2 and Supporting Information Figure S2). It was observed that some of these precursors harbored the long "stem" regions producing the AGO1-enriched sRNAs (Figure 2E), which were reminiscent of the young miRNAs evolved from gene inverted duplication events or miniature inverted-repeat transposable elements (Allen et al. 2004; Cuperus et al. 2011; Piriyapongsa and Jordan 2008). Besides, some of the mature miRNA candidates were organ-specifically expressed (Figure 2C,D,F and Supporting Information Figure S2), indicating their spatio-temporal regulatory activities.

In plants, guided by the sRNAs, the AGO1-centered RISCs bind onto the complementary SBSs for target cleavage. In addition to miRNAs, ta-siRNAs, and vsiRNAs (Fang and Qi 2016; Fei et al. 2013; Jones-Rhoades et al. 2006; Yu et al. 2026), we were curious whether this kind of regulation involved some other unannotated sRNAs also enriched in AGO1. The canonical method for SBS identification is direct submission of the query transcripts to the bioinformatics tools for complementary region prediction. In the present study, AGO1-RIP-RNA-seq was employed for the transcriptome-wide identification of the AGO1 binding regions. By focusing on the SBSs covered by the AGO1 RIP peaks, the predicted sRNA targets without AGO1 binding signals was removed, thus reducing the false positive rate of target predictions. Indeed, degradome-based SBS validation showed that a significant portion of the sRNA–target pairs detected in WT were AGO1-dependent, as compared to the *ago1* mutants. Especially in *ago1-27*, 437 out of 456 pairs (95.83%) were observed to be AGO1-dependent (Figure 3A). Thus, both the high AGO1 dependency of the sRNA–target pairs and the experimental evidence provided by 5′RACE (Figure 3F and Supporting Information Figure S4) demonstrates the power of combinatory use of the AGO1-RIP-RNA-seq data and the degradome-seq data for identification of the targetomes regulated by the AGO1-enriched sRNAs.

We performed statistical analysis of the RIP-seq data used in this study. Specifically, for the two biological replicates of AGO1-RIP-seq performed after rRNA removal, 3956 and 5852 peaks were identified, respectively ($p < 0.01$) (Supporting Information Table S2). However, only 346 peaks (8.75%) in replicate 1 were observed to be overlapped (≥ 80% overlapping region for each peak pair) with 349 peaks (5.96%) in replicate 2. The reproducibility between the two runs of AGO1-RIP-seq is lower than ideal, which may attribute to the following points. First of all, it is well known that AGO1, sRNAs and target RNAs form extremely unstable ternary complexes in *Arabidopsis*, since a large portion of the target transcripts will be immediately sliced upon AGO1–sRNA recognition (Carbonell 2017). In other words, the RNA fragments bound by AGO1 are highly dynamic and difficult to capture due to their elusive abundances. Understanding the dynamics of AGO1–sRNA–target interactions is important for the mechanistic studies on plant RNAi (Carbonell 2017; Fang and Qi 2016). Second, in *Arabidopsis*, AGO1 is implicated in diverse molecular processes such

FIGURE 5 | Identification and characterization of the organ- and temperature-specific targetomes. (A) Networks showing the degradome-supported sRNA–target pairs specifically identified from flowers, leaves, roots, and seedlings. Under 15°C treatment, 183, 133, 299, and 353 pairs were specifically identified from the four samples, respectively. Under 21°C, 297, 214, 375, and 247 organ-specific pairs were identified. Under 27°C, 283, 284, 341, and 215 organ-specific pairs were identified. (B) Networks showing the degradome-supported sRNA–target pairs identified under specific temperature treatments. In flowers, 143, 239, and 256 pairs were specifically identified under 15°C, 21°C, and 27°C, respectively. In leaves, 101, 164, and 273 pairs were specifically identified under 15°C, 21°C, and 27°C, respectively. In roots, 233, 250, and 243 pairs were specifically identified under 15°C, 21°C, and 27°C, respectively. In seedlings, 483, 216, and 198 pairs were specifically identified under 15°C, 21°C, and 27°C, respectively. (C) In-depth analysis of the degradome-supported sRNA–target pairs identified from distinct organs under different temperature treatments. Metagene profiles show the distribution patterns of the degradome-supported SBSs and the AGO1 RIP peaks covering these SBSs. The results of GO (Gene Ontology) term enrichment analyses (hypergeometric test, $p < 0.01$; the top 10 GO terms were selected) are also shown for the taget genes (the GO terms related to organ development were highlighted in red). For each GO term, the Q values (< 0.1) calculated by the Benjamini–Hochberg procedure is also shown (in red) adjacent to the bubble for reference. [Color figure can be viewed at wileyonlinelibrary.com]

13653040, 0, Downloaded from https://onlinelibrary.wiley.com/doi/10.1111/pce.70893 by Yijun Meng - Hangzhou Normal University , Wiley Online Library on [16/09/2026]. See the Terms and Conditions (https://onlinelibrary.wiley.com/terms-and-conditions) on Wiley Online Library for rules of use; OA articles are governed by the applicable Creative Commons License

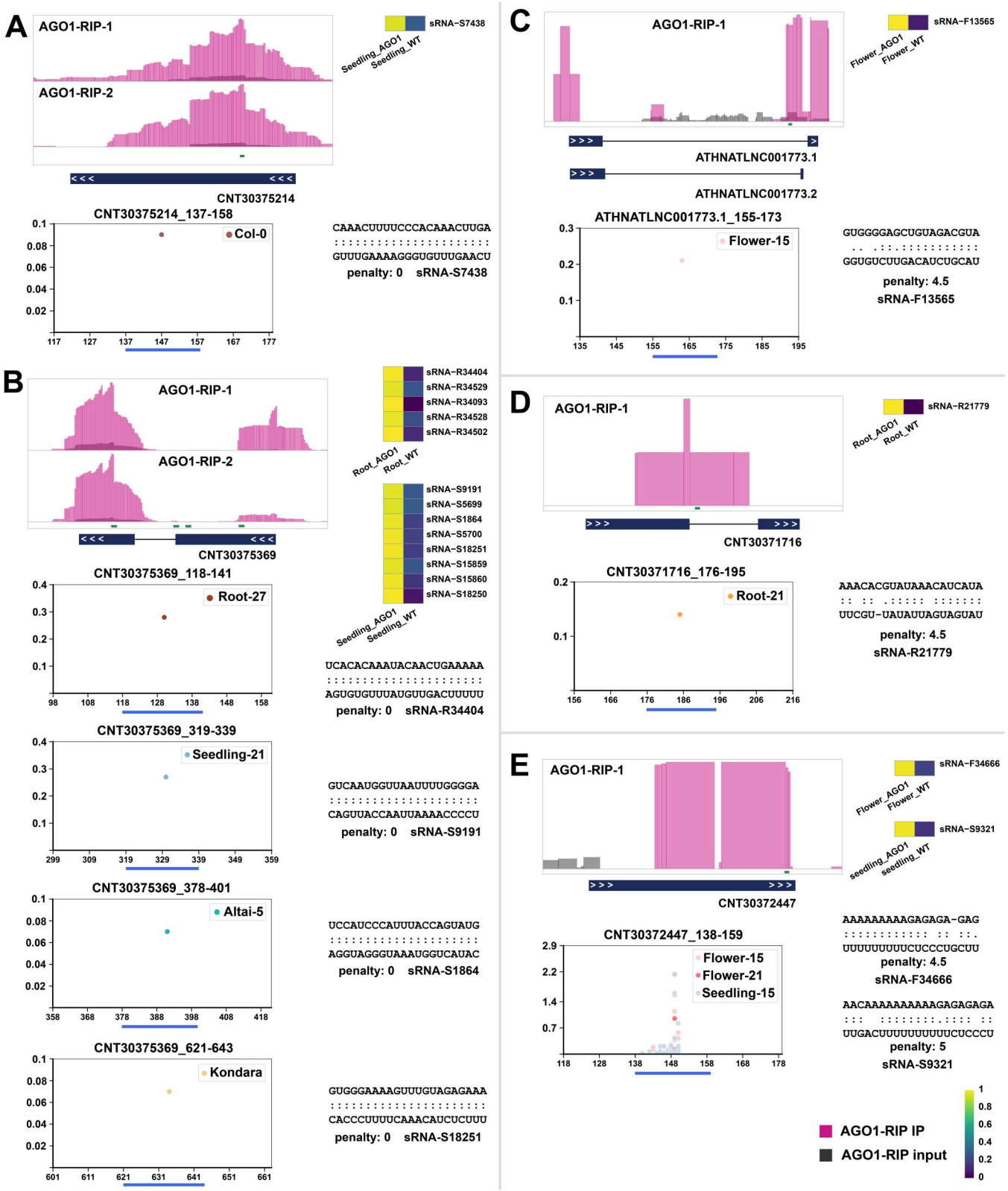


FIGURE 6 | Examples of the long non-coding RNAs (lncRNAs) targeted by the AGO1-enriched sRNAs. For each case (from A to E), the IGV window shows the AGO1 binding signals on the target transcript based on the AGO1-RIP-RNA-seq data (the SBS was indicated by a short green bar). The target plots (t-plots) presenting the degradome signatures mapped onto the target transcript provides the evidence of sRNA-guided cleavage (*x* axes indicating the positions on the target transcripts; *y* axes measuring the levels of the degradome signals in RPM, reads per million). The heatmaps show the evidence of the AGO1 enrichment for the regulatory sRNAs. [Color figure can be viewed at wileyonlinelibrary.com]

13653040, 0, Downloaded from https://onlinelibrary.wiley.com/doi/10.1111/pce.70893 by Yijun Meng - Hangzhou Normal University , Wiley Online Library on [16/09/2026]. See the Terms and Conditions (https://onlinelibrary.wiley.com/terms-and-conditions) on Wiley Online Library for rules of use; OA articles are governed by the applicable Creative Commons License

as target cleavages, translational repression, and RNA splicing (Fang and Qi 2016; Li et al. 2022; Liang et al. 2023; Meng et al. 2022), which leads to massive binding sites on the target transcripts. Third, based on IP-MS (immunoprecipitation followed by mass spectrometry), our previous result showed that several mRNA binding factors interacted with AGO1 in *Arabidopsis* (Meng et al. 2022), which might greatly expand the direct and indirect target repository of AGO1. To rule out the possibility that the poor reproducibility was caused by technical factors, we performed another AGO1-RIP-seq experiment performed without rRNA removal. Due to the interference by rRNA reads, the valid reads were greatly reduced. As a result, only 412 and 276 peaks were identified for the two biological replicates, respectively ($p < 0.01$) (Supporting Information Table S2). But notably, 139 (33.74%) in replicate 1 were observed to be overlapped with 136 (49.28%) in replicate 2. The significantly elevated ratios of the overlapping peaks indicated that our RIP-seq experiments were technically sound. The discrepancy between "rRNA removal" and "without rRNA removal" might be explained by the massive but elusive trace signals which could be dynamically detectable after rRNA removal but would be masked by the dominant rRNA reads. Besides, as shown by the IP results of the RIP-seq experiments, the target protein bands (AGO1: ~130 kDa; HYL1: ~68 kDa) were detectable in both "input" and "IP" samples, and the signals were especially stronger in the "IP" samples. But for "IgG control," the target protein bands could be hardly detected (Supporting Information Figure S1), indicating the specificity of our IP experiments. Thus, use of the overlapping RIP peaks between the two replicates will result in a substantial loss of the potential targets of AGO1-associated sRNAs. Degradome-seq is a powerful method for high-throughput mapping of the sRNA-guided slicing sites in the target transcripts (German et al. 2008). However, degradome-seq cannot distinguish which specific AGO member performs its regulation. Facilitated by AGO1-RIP-seq, the researchers can specifically focus on the AGO1-regulated targets. It is foreseeable that the application of RIP-seq to different AGOs can reveal the specific target pool regulated by each AGO protein in *Arabidopsis*. Taken together, the union of the two replicates of AGO1-RIP-seq was used for this study based on the two points: (1) AGO1-RIP-seq was an auxiliary tool for sRNA target identification, and the targets would be finally validated by degradome-seq data or modified 5′RACE; (2) the AGO1 binding signals were elusive trace signals, and use of the intersection of the two replicates will result in a substantial loss of the potential targets.

Previous studies showed that a great portion of the genes targeted by miRNAs were functionally implicated in transcriptional regulation (Jones-Rhoades et al. 2006), which was also observed by GO term enrichment analysis of the sRNA targetome identified from the WT seedlings in the present study (Figure 3B). However, more and more recent studies found that the majority of the miRNA targets were not transcription factors (Alves-Junior et al. 2009). Thus, it is intriguing to examine the biological functions of the genes targeted by the AGO1-enriched sRNAs. By analyzing the targetomes identified from different ecotypes and organs of *Arabidopsis*, a substantial part were discovered to be environment-responsive and organ-specific, respectively (Figures 4 and 5C). This result indicates that in addition to miRNAs, some of the other sRNA species enriched in AGO1 may have more extensive biological functions than imagined.

We acknowledged that in the present study, identification of the temperature-specific targetomes is a case study lacking a fully comprehensive set of temperature-specific RIP-seq data. Ideally, the interactions between AGO1 and target transcripts should be detected by using the RIP-seq data under the specific temperature treatments consistent with those for the degradome-seq experiments. However, the case study was performed based on the scenario that the interactions between AGO1 and its targets, in most cases, are a matter of quantitative change rather than qualitative change under different temperature treatments. Indeed, some of the potential interactions detected by the RIP-seq data under 24°C were successfully validated by the degradome data under specific temperature treatments. To understand the detailed molecular mechanisms underlying temperature-specific regulation, it will be interesting to investigate the temperature effects on AGO1–target interactions by direct using the RIP-seq data under the specific temperature treatments in future studies. Of course, it also needs to examine the temperature effects on the expression levels of *AGO1* and other related genes.

Most of the previous studies on the regulatory relationship between lncRNAs and sRNAs focused on the role of lncRNAs as the endogenous target mimics in reducing miRNA activities (Franco-Zorrilla et al. 2007; Y. J. Meng et al. 2012; Wu et al. 2013; X. P. Zhang et al. 2021). Limited cases, such as the production of ta-siRNAs through miRNA-mediated cleavage of the *TAS* transcripts (H. M. Chen et al. 2007; de Felippes et al. 2017; Felippes and Weigel 2009), were related to the regulation of lncRNAs by sRNAs. In the present study, some of the AGO1-enriched sRNAs showed the great potential of regulating the lncRNA targets (Figure 6 and Supporting Information Figure S6), which advanced our understanding of the regulatory function of the AGO1-enriched sRNAs.

In the present study, the RIP-RNA-seq datasets of HYL1 and AGO1 were limited to the WT seedlings. However, it is foreseeable that diversified sampling for RIP-seq library preparation will enlarge the repository of the miRNA precursor candidates, or expand the sRNA targetomes. For example, construction of the AGO1-RIP-RNA-seq library of the slicer-defective mutant(s) in which the AGO1–sRNA–target ternary complexes are not disrupted (Carbonell et al. 2012) should lead to the discovery of much more SBSs. Summarily, our study has shown the power of integrated RIP-seq data analysis for identification of the AGO1-enriched sRNomes and targetomes in plants.

5 | Conclusion

The results of the present study emphasized the utility of integrated analysis of the RIP-seq data in identification of the AGO1-enriched sRNomes and their targetomes. Assisted by the RIP-RNA-seq of HYL1 and DCL1, two key factors for miRNA maturation, further exploration of the sRNAs enriched in the AGO1-centered silencing complexes enabled us to discover the novel miRNA candidates in *Arabidopsis*. On the other hand, functional analysis of the ecotype- and organ-specific target

13653040, 0, Downloaded from https://onlinelibrary.wiley.com/doi/10.1111/pce.70893 by Yijun Meng - Hangzhou Normal University , Wiley Online Library on [16/09/2026]. See the Terms and Conditions (https://onlinelibrary.wiley.com/terms-and-conditions) on Wiley Online Library for rules of use; OA articles are governed by the applicable Creative Commons License

genes provided valuable biological hints related to environmental responses and developmental processes of *Arabidopsis*. Summarily, our workflow proposed here should be useful for plant sRNA studies.

Acknowledgements

We thank Yijun Qi (School of Life Sciences, Tsinghua University) for providing the mutants *ago1-25* and *ago1-27*. We thank Hidetaka Ito (Faculty of Science, Hokkaido University) for providing the different ecotypes of *Arabidopsis* (Col-0, Altai-5, ICE73, Kas-2, Kondara, Se-0, and Zal-1). This study was supported by grants from the National Natural Science Foundation of China [32370707] and [32070655].

Conflicts of Interest

The authors declare no conflicts of interest.

Data Availability Statement

The data that support the findings of this study are available in the Supporting Information of this article.

References

Allen, E., Z. Xie, A. M. Gustafson, G. H. Sung, J. W. Spatafora, and J. C. Carrington. 2004. "Evolution of microRNA Genes by Inverted Duplication of Target Gene Sequences in *Arabidopsis thaliana*." *Nature Genetics* 36, no. 12: 1282–1290.

Alves-Junior, Jr., L., S. Niemeier, A. Hauenschild, M. Rehmsmeier, and T. Merkle. 2009. "Comprehensive Prediction of Novel microRNA Targets in *Arabidopsis thaliana*." *Nucleic Acids Research* 37, no. 12: 4010–4021.

Bolger, A. M., M. Lohse, and B. Usadel. 2014. "Trimmomatic: A Flexible Trimmer for Illumina Sequence Data." *Bioinformatics* 30, no. 15: 2114–2120.

Bologna, N. G., A. Sarazin, and G. Schott, et al. 2026. "Transcriptome-Wide Analysis of *Arabidopsis* DICER-LIKE1 RNA Substrates." *Nucleic Acids Research* 54, no. 3: gkaf1434.

Carbonell, A. 2017. "Plant ARGONAUTEs: Features, Functions, and Unknowns." *Methods in Molecular Biology* 1640: 1–21.

Carbonell, A., N. Fahlgren, H. Garcia-Ruiz, et al. 2012. "Functional Analysis of Three *Arabidopsis* ARGONAUTES Using Slicer-Defective Mutants." *Plant Cell* 24, no. 9: 3613–3629.

Chen, H. M., Y. H. Li, and S. H. Wu. 2007. "Bioinformatic Prediction and Experimental Validation of a microRNA-Directed Tandem *trans*-Acting siRNA Cascade in *Arabidopsis*." *Proceedings of the National Academy of Sciences* 104, no. 9: 3318–3323.

Chen, X. 2009. "Small RNAs and Their Roles in Plant Development." *Annual Review of Cell and Developmental Biology* 25: 21–44.

Cuperus, J. T., N. Fahlgren, and J. C. Carrington. 2011. "Evolution and Functional Diversification of *MIRNA* Genes." *Plant Cell* 23, no. 2: 431–442.

Dobin, A., C. A. Davis, F. Schlesinger, et al. 2013. "STAR: Ultrafast Universal RNA-Seq Aligner." *Bioinformatics* 29, no. 1: 15–21.

Fahlgren, N., and J. C. Carrington. 2010. "miRNA Target Prediction in Plants." *Methods in Molecular Biology* 592: 51–57.

Fang, X., and Y. Qi. 2016. "RNAi in Plants: An Argonaute-Centered View." *Plant Cell* 28, no. 2: 272–285.

Fei, Q., R. Xia, and B. C. Meyers. 2013. "Phased, Secondary, Small Interfering RNAs in Posttranscriptional Regulatory Networks." *Plant Cell* 25, no. 7: 2400–2415.

de Felippes, F. F., A. Marchais, A. Sarazin, S. Oberlin, and O. Voinnet. 2017. "A Single miR390 Targeting Event Is Sufficient for Triggering *TAS3*-tasiRNA Biogenesis in *Arabidopsis*." *Nucleic Acids Research* 45, no. 9: 5539–5554.

Felippes, F. F., and D. Weigel. 2009. "Triggering the Formation of tasiRNAs in *Arabidopsis thaliana*: The Role of microRNA miR173." *EMBO Reports* 10, no. 3: 264–270.

Feng, Z., X. Ma, X. Wu, et al. 2024. "Genome-Wide Identification of phasiRNAs in *Arabidopsis thaliana*, and Insights Into Biogenesis, Temperature Sensitivity, and Organ Specificity." *Plant, Cell & Environment* 47, no. 10: 3797–3812.

Feng, Z., J. Yao, Z. Jiang, et al. 2026. "DNA Polymorphisms and N^6-Methyladenosine RNA Methylation Influencing microRNA Expression and Regulatory Activity in Plants." *BMC Plant Biology* 26, no. 1: 675.

Franco-Zorrilla, J. M., A. Valli, M. Todesco, et al. 2007. "Target Mimicry Provides a New Mechanism for Regulation of microRNA Activity." *Nature Genetics* 39, no. 8: 1033–1037.

Frank, F., J. Hauver, N. Sonenberg, and B. Nagar. 2012. "Arabidopsis Argonaute MID Domains Use Their Nucleotide Specificity Loop to Sort Small RNAs." *EMBO Journal* 31, no. 17: 3588–3595.

Alonso-Blanco, C., J. Andrade, C. Becker, et al. 2016. "1,135 Genomes Reveal the Global Pattern of Polymorphism in *Arabidopsis thaliana*." *Cell* 166: 481–491.

German, M. A., M. Pillay, D. H. Jeong, et al. 2008. "Global Identification of microRNA-Target RNA Pairs by Parallel Analysis of RNA Ends." *Nature Biotechnology* 26, no. 8: 941–946.

Gyula, P., I. Baksa, T. Tóth, I. Mohorianu, T. Dalmay, and G. Szittya. 2018. "Ambient Temperature Regulates the Expression of a Small Set of sRNAs Influencing Plant Development Through NF-YA2 and YUC2." *Plant, Cell & Environment* 41, no. 10: 2404–2417.

Jones-Rhoades, M. W., D. P. Bartel, and B. Bartel. 2006. "MicroRNAs and Their Regulatory Roles in Plants." *Annual Review of Plant Biology* 57: 19–53.

Kozomara, A., M. Birgaoanu, and S. Griffiths-Jones. 2019. "miRBase: From microRNA Sequences to Function." *Nucleic Acids Research* 47, no. D1: D155–D162.

Li, Z., W. Li, M. Guo, et al. 2022. "Origin, Evolution and Diversification of Plant ARGONAUTE Proteins." *Plant Journal* 109, no. 5: 1086–1097.

Liang, C., X. Wang, H. He, C. Xu, and J. Cui. 2023. "Beyond Loading: Functions of Plant ARGONAUTE Proteins." *International Journal of Molecular Sciences* 24, no. 22: 16054.

Llave, C., Z. Xie, K. D. Kasschau, and J. C. Carrington. 2002. "Cleavage of *Scarecrow-Like* mRNA Targets Directed by a Class of *Arabidopsis* miRNA." *Science* 297, no. 5589: 2053–2056.

Lorenz, R., S. H. Bernhart, C. Höner zu Siederdissen, et al. 2011. "ViennaRNA Package 2.0." *Algorithms for Molecular Biology* 6: 26.

Lyu, F., F. Han, C. Ge, et al. 2023. "OmicStudio: A Composable Bioinformatics Cloud Platform With Real-Time Feedback That Can Generate High-Quality Graphs for Publication." *Imeta* 2, no. 1: e85.

Mallory, A. C., D. P. Bartel, and B. Bartel. 2005. "MicroRNA-Directed Regulation of Arabidopsis *AUXIN RESPONSE FACTOR*$_{17}$ Is Essential for Proper Development and Modulates Expression of Early Auxin Response Genes." *Plant Cell* 17, no. 5: 1360–1375.

Mason, G. A., T. Lemus, and C. Queitsch. 2016. "The Mechanistic Underpinnings of an ago1-Mediated, Environmentally Dependent, and Stochastic Phenotype." *Plant Physiology* 170: 2420–2431.

Meng, J., Z. Lu, H. Liu, et al. 2014. "A Protocol for RNA Methylation Differential Analysis With MeRIP-Seq Data and exomePeak R/Bioconductor Package." *Methods* 69, no. 3: 274–281.

Meng, Y., X. Ma, J. Li, et al. 2022. "The Novel Activity of Argonautes in Intron Splicing: A Transcriptome-Wide Survey in Plants." *Journal of Plant Physiology* 270: 153632.

13653040, 0, Downloaded from https://onlinelibrary.wiley.com/doi/10.1111/pce.70893 by Yijun Meng - Hangzhou Normal University , Wiley Online Library on [16/09/2026]. See the Terms and Conditions (https://onlinelibrary.wiley.com/terms-and-conditions) on Wiley Online Library for rules of use; OA articles are governed by the applicable Creative Commons License

Meng, Y., C. Shao, and M. Chen. 2011. "Toward microRNA-Mediated Gene Regulatory Networks in Plants." *Briefings in Bioinformatics* 12, no. 6: 645–659.

Meng, Y., C. Shao, H. Wang, and Y. Jin. 2012. "Target Mimics: An Embedded Layer of microRNA-Involved Gene Regulatory Networks in Plants." *BMC Genomics* 13: 197.

Mi, S., T. Cai, Y. Hu, et al. 2008. "Sorting of Small RNAs Into *Arabidopsis* Argonaute Complexes Is Directed by the 5′ Terminal Nucleotide." *Cell* 133, no. 1: 116–127.

Montgomery, T. A., M. D. Howell, J. T. Cuperus, et al. 2008. "Specificity of ARGONAUTE7-miR390 Interaction and Dual Functionality in *TAS3 trans*-Acting siRNA Formation." *Cell* 133, no. 1: 128–141.

Piriyapongsa, J., and I. K. Jordan. 2008. "Dual Coding of siRNAs and miRNAs by Plant Transposable Elements." *RNA* 14, no. 5: 814–821.

Quinlan, A. R., and I. M. Hall. 2010. "BEDTools: A Flexible Suite of Utilities for Comparing Genomic Features." *Bioinformatics* 26, no. 6: 841–842.

Reiser, L., E. Bakker, and S. Subramaniam, et al. 2024. "The Arabidopsis Information Resource in 2024." *Genetics* 227, no. 1: iyae027.

Sánchez-García, A. B., V. Aguilera, R. Micol-Ponce, S. Jover-Gil, and M. R. Ponce. 2015. "ArabidopsisMAS2, an Essential Gene That Encodes a Homolog of Animal NF-κ B Activating Protein, Is Involved in 45S Ribosomal DNA Silencing." *Plant Cell* 27: 1999–2015.

Shannon, P., A. Markiel, O. Ozier, et al. 2003. "Cytoscape: A Software Environment for Integrated Models of Biomolecular Interaction Networks." *Genome Research* 13, no. 11: 2498–2504.

Shao, C., M. Chen, and Y. Meng. 2013. "A Reversed Framework for the Identification of microRNA-Target Pairs in Plants." *Briefings in Bioinformatics* 14, no. 3: 293–301.

Stief, A., S. Altmann, K. Hoffmann, B. D. Pant, W. R. Scheible, and I. Bäurle. 2014. "Arabidopsis miR156 Regulates Tolerance to Recurring Environmental Stress Through SPL Transcription Factors." *Plant Cell* 26: 1792–1807.

Szcześniak, M. W., and E. Wanowska (2024). CANTATAdb 3.0: An Updated Repository of Plant Long Non-Coding RNAs. Plant and Cell Physiology, 65(9), 1486–1493.

Thorvaldsdottir, H., J. T. Robinson, and J. P. Mesirov. 2013. "Integrative Genomics Viewer (IGV): High-Performance Genomics Data Visualization and Exploration." *Briefings in Bioinformatics* 14, no. 2: 178–192.

Vaucheret, H. 2008. "Plant ARGONAUTES." *Trends in Plant Science* 13, no. 7: 350–358.

Vaucheret, H., F. Vazquez, P. Crété, and D. P. Bartel. 2004. "The Action of ARGONAUTE1 in the miRNA Pathway and Its Regulation by the miRNA Pathway Are Crucial for Plant Development." *Genes & Development* 18, no. 10: 1187–1197.

Wang, H., X. Zhang, J. Liu, et al. 2011. "Deep Sequencing of Small RNAs Specifically Associated With *Arabidopsis* AGO1 and AGO4 Uncovers New AGO Functions." *Plant Journal* 67, no. 2: 292–304.

Wierzbicki, A. T., T. Blevins, and S. Swiezewski. 2021. "Long Noncoding RNAs in Plants." *Annual Review of Plant Biology* 72: 245–271.

Wu, H. J., Z. M. Wang, M. Wang, and X. J. Wang. 2013. "Widespread Long Noncoding RNAs as Endogenous Target Mimics for MicroRNAs in Plants." *Plant Physiology* 161, no. 4: 1875–1884.

Xiao, Y., and I. J. MacRae. 2022. "The Molecular Mechanism of microRNA Duplex Selectivity of *Arabidopsis* ARGONAUTE10." *Nucleic Acids Research* 50, no. 17: 10041–10052.

Xu, J., E. Shen, F. Guo, et al. 2025. "Identification of Cell-Type Specificity, trans- and cis-Acting Functions of Plant lincRNAs From Single-Cell Transcriptomes." *New Phytologist* 245, no. 2: 698–710.

Yu, Y., H. Wang, C. You, and X. Chen. 2026. "Plant microRNA Maturation and Function." *Nature Reviews Molecular Cell Biology* 27, no. 1: 55–70.

Zhang, H., R. Xia, B. C. Meyers, and V. Walbot. 2015. "Evolution, Functions, and Mysteries of Plant ARGONAUTE Proteins." *Current Opinion in Plant Biology* 27: 84–90.

Zhang, L., S. Chen, X. Chen, X. Du, and H. Liu. 2022. "Guitar2: An Improved Version of the Guitar for Sketching the Transcriptomic View of RNA-Related Biological Features." *Methods* 203: 40–45.

Zhang, X., D. Niu, A. Carbonell, et al. 2014. "ARGONAUTE PIWI Domain and microRNA Duplex Structure Regulate Small RNA Sorting in *Arabidopsis*." *Nature Communications* 5: 5468.

Zhang, X., J. Shen, Q. Xu, et al. 2021. "Long Noncoding RNA lncRNA354 Functions as a Competing Endogenous RNA of miR160b to Regulate *ARF* Genes in Response to Salt Stress in Upland Cotton." *Plant, Cell & Environment* 44, no. 10: 3302–3321.

Supporting Information

Additional supporting information can be found online in the Supporting Information section.

Supporting File 1: pce70893-sup-0001-Figure_S1.pdf.
Supporting File 2: pce70893-sup-0002-Figure_S2.pdf.
Supporting File 3: pce70893-sup-0003-Figure_S3.pdf.
Supporting File 4: pce70893-sup-0004-Figure_S4.pdf.
Supporting File 5: pce70893-sup-0005-Figure_S5.pdf.
Supporting File 6: pce70893-sup-0006-Figure_S6.pdf.
Supporting File 7: pce70893-sup-0007-Supplementary_Tables.zip.
Supporting File 8: pce70893-sup-0008-Supplementary-data_instructions.doc.

13653040, 0, Downloaded from https://onlinelibrary.wiley.com/doi/10.1111/pce.70893 by Yijun Meng - Hangzhou Normal University , Wiley Online Library on [16/09/2026]. See the Terms and Conditions (https://onlinelibrary.wiley.com/terms-and-conditions) on Wiley Online Library for rules of use; OA articles are governed by the applicable Creative Commons License